Characterisation of D6AC Steel Using A Unified Constitutive Model

A. Searl and J. Paul

DSTO-TR-0556

19971007 203

DEPARTMENT ♦ OF DEFENCE

DEFENCE SCIENCE AND TECHNOLOGY ORGANISATION

Characterisation of D6AC Steel Using A Unified Constitutive Model

A.Searl and J. Paul

Airframes and Engines Division
Aeronautical and Maritime Research Laboratory

DSTO-TR-0556

ABSTRACT

An experimental test program was undertaken to characterise the inelastic response of D6ac steel under differing cyclic loading. A unified constitutive model was used to describe material behaviour. Constants for the model were extracted from the test results and numerical model predictions were compared with the experimental results. The tests revealed that D6ac steel saturates after one cyclic loop and a change in modulus was observed after unloading from a tensile load. Also described are improvements in the testing of uniaxial specimens, focusing on techniques for specimen alignment to minimise out of plane bending effects.

RELEASE LIMITATION

Approved for public release

D E P A R T M E N T   O F   D E F E N C E

◆

DEFENCE SCIENCE AND TECHNOLOGY ORGANISATION

Characterisation of D6AC Steel Using A Unified Constitutive Model

Executive Summary

Every 7 years the F-111 Aircraft undergoes a Cold Proof Load Test (CPLT) as part of the Structural Integrity Program. During this loading, local regions of the Wing Pivot Fitting experience a high level of plastic deformation. A consequence of particular concern is that the Fuel Flow Vent Hole Number 13 (FFVH#13) experiences fatigue cracking due to the residual stresses which are left in the structure after the CPLT cycle. The Royal Australian Air Force (RAAF) manages the structural integrity of its F-111 fleet by safety by inspection, with inspection intervals derived from a durability and damage tolerance analyses (DADTA). As part of the calculation of the inspection interval for FFVH#13, a detailed knowledge of the residual stress field imposed by a single CPLT cycle is required. AMRL's role is to accurately determine the elastic and cyclic residual stresses as input to this DADTA.

Recent full scale wing tests conducted at AMRL indicate that at peak load the lower inboard corner of FFVH#13, where instances of cracking have occurred, experiences strain levels three times that of yield. To accurately analyse the effects of such high strain levels, a Finite Element analysis of the critical region was required. This analysis must correctly represent the material behaviour under the non-symmetric cyclic loads. Classical plasticity models have inherent difficulties when dealing with cyclic loading and therefore alternative methods have been employed. One such method used at AMRL is a state variable constitutive material approach, originally developed by Ramaswamy, Stouffer and Bodner, and subsequently jointly enhanced by AMRL, the University of Melbourne and Monash University over recent years.

This report describes an experimental test program which characterises the inelastic response of D6ac steel under differing cyclic loading. Unified constitutive material model constants were extracted from the test results and refined using a FORTRAN program which represents the uniaxial test condition. These refined constants when applied to the constitutive model successfully predicted the behaviour of D6ac steel under different cyclic loading conditions including the CPLT cycle.

This constitutive model forms part of the input to the Finite Element solutions used in the detailed plasticity analyses of the F-111 FFVH#13. The elastic and residual stress fields found in this analyses will then be used in the DADTA as an important ingredient in determining the inspection interval for this critical location.

Authors

A. Searl
Airframes and Engines Division

Mr Searl has a degree in Aerospace Engineering having graduated from RMIT in 1994 with first class honours, and is currently studying for a doctor of philosophy in Aerospace Engineering at RMIT as a Cadet Research Scientist. Since commencing work with AMRL in 1995, he has been involved with the finite element modelling and analysis of the Fuel Flow Vent Hole #13 location in the F-111C Wing Pivot Fitting, and the investigation of composite bonded reinforcements for the F/A-18 fuselage bulkhead re-entrant corner. His current research involves investigation into the structural optimisation of complex composite structures for the CRC-AS and AMRL.

J. Paul
Airframes and Engines Division

Mr Paul has a degree in Aeronautical Engineering and a Masters in Mechanical Engineering in the repair of thick composite structures. He has worked in the finite element field for 13 years providing AMRL with a high level of expertise in the area of computational analysis which has been utilised to solve a variety of RAAF related stress/strain problems seen on the F-111C and F/A-18 aircraft. He is currently the Functional Head of the Computational Stress Analysis Facilities within AED and leads the team working on the F-111C Structural Integrity Task, which provides the residual stress input required for the calculation of the inspection interval for the Fuel Flow Vent Hole #13 location in the F-111C Wing Pivot Fitting.

Contents

1. Introduction

The Aeronautical and Maritime Research Laboratory (AMRL) has the key role of supporting the Royal Australian Air Force (RAAF) in the structural integrity management of its fleet of F-111 aircraft. As a part of the fatigue life enhancement of the F-111, the original manufacturer developed a testing procedure to detect cracks in components of the aircraft that were made from D6ac steel. D6ac is a high strength steel, and as a consequence has an extremely low critical crack length. This characteristic poses problems with regards to the fatigue life monitoring of the aircraft. Many critical areas of the F-111 are difficult to access with non-destructive inspection (NDI) equipment, making it impractical to detect cracking by normal inspection methods. Cold proof Load Testing (CPLT) is the testing procedure developed to overcome the complications presented by the F-111 and D6ac steel. Basically the CPLT consists of first cooling the aircraft to -40°F, where the fracture toughness of D6ac steel is significantly lower than at room temperature, and then applying a limit loading cycle to the aircraft. If the aircraft survives CPLT it is considered safe for a further period of time, before any cracks present during CPLT grow to significant length. After this period of time the aircraft undergoes another CPLT program.

An undesirable side-effect of the CPLT program is that compressive yielding at stress concentrators in the upper plate of the wing pivot fitting (WPF) leaves localised tensile stresses which facilitate the initiation and growth of fatigue cracks under subsequent service loading. One such area of particular concern is that of Fuel Flow Vent Hole (FFVH) #13. The RAAF manages the structural integrity of its F-111 fleet through safety by inspection, with inspection intervals derived from durability and damage tolerance analyses (DADTA). The DADTA on which the current inspection interval for FFVH#13 is based took some account of the residual stresses by imposing a single CPLT load at the start of crack growth calculations. The RAAF now requires a DADTA of FFVH#13 to be performed incorporating an accurate representation of the residual stresses. AMRL's role is to determine the material response for input to this DADTA, which is conducted under contract from the RAAF. The work described in this report forms part of that broader AMRL work programme of which an overview is given in [1].

Recent full scale wing test data [2] indicate that the lower inboard corner of FFVH#13, where instances of cracking have occurred, experiences strain levels ranging from 18,000 to 22,000 microstrain ($\mu\varepsilon$). The yield strain of D6ac is approximately 7000$\mu\varepsilon$, so this illustrates the high degree of plasticity being exhibited by this region of the structure at peak load. To accurately analyse the effects of such high strain levels under CPLT, a Finite Element Model (FEM) of the FFVH#13 region is being employed. To predict the residual stress left after a CPLT application, a non-linear FEM solution must be performed. Given the cyclic nature of the CPLT application, and the inadequacy of classical plasticity models in predicting inelastic cyclic response, a constitutive model was employed to describe the inelastic behaviour of the material. This constitutive model applies a state variable, rate dependent approach which allows

1

accurate modelling of the deformation history of the material experienced during cyclic loading. The Finite Element package being used for this analysis is PAFEC, which has the built in ability to analyse non-linear material problems. The standard material models in PAFEC only make use of classical techniques for modelling plasticity, however PAFEC does allow the capability of applying user written routines such as alternative plasticity models.

State variable constitutive modelling has been used to improve predictions of the cyclic stress condition in materials. The state variable approach to the modelling of cyclic plasticity attempts to model the micro structural deformation of the material experienced during the application of cyclic loading. This attribute results in a more accurate prediction of the material behaviour. The constitutive model being employed for this work is based on that created by Ramaswamy, Stouffer and Bodner [3], which has been subsequently jointly enhanced by AMRL, Melbourne University and Monash University over recent years. [4,5,6]

To develop the material parameters for the initial prediction of the state variable inelastic constitutive model, sets of uniaxial experimental data for D6ac steel were required. This report describes a series of uniaxial tension/compression tests performed to characterise the material behaviour of D6ac steel under cyclic inelastic loading. These data sets were then used to determine the initial values of the unified constitutive model's material constants. This first estimate was refined using a FORTRAN computer program which represents the uniaxial testing condition using the unified constitutive equations.

In a parallel program of work, the theoretical and analytical solution techniques of the unified constitutive model were developed in references 3, 5 and 6. The implementation of the analysis software into the PAFEC finite element program can be found in references 4 and 7. The achievements of this work now make it possible to perform the required plasticity analysis, accurately and efficiently. This capability is being used on the F-111C FFVH#13 problem to solve for the large cyclic plastic strains that occur during the CPLT.

2. Theory

The unified constitutive model developed by Ramaswamy, Stouffer and Bodner [3] consists of the inelastic flow equation and the rate forms of the state variables; back stress Ω_{ij}, and drag stress Z. The drag stress, Z, is taken as a scalar value as its evolution (interaction of dislocations with subgrains, cells, precipitates, etc) is largely orientation independent [8]. Equations for the multiaxial form of the unified constitutive model are:

$$\dot{\varepsilon}_{ij}^{I} = D \exp\left[-\frac{1}{2}\left(\frac{Z^2}{3K_2}\right)^n\right]\frac{\left(S_{ij}-\Omega_{ij}\right)}{\sqrt{K_2}} \tag{1}$$

where $\dot{\varepsilon}_{ij}^I$ is the inelastic strain rate, K_2 is the second invariant of the inelastic strain rate tensor, S_{ij} is the deviatoric stress tensor, and D and n are temperature and strain rate dependent material parameters. For D6ac steel, at room temperature, D=10000 for tensile and fatigue responses (for strain rates up to 1.0 sec^{-1}), and n=3 for strain rate insensitivity. Here the evolution equation for the back stress Ω_{ij} is defined as:

$$\Omega_{ij} = f_2 S_{ij} + \Omega_{ij}^I \qquad (2)$$

where f_2 is a material parameter and S_{ij} is the deviatoric stress tensor. The inelastic back stress Ω_{ij}^I is calculated by integrating the following,

$$\dot{\Omega}_{ij}^I = \frac{2}{3} f_1 \dot{\varepsilon}_{eff}^I - f_1 \frac{\Omega_{ij}}{\Omega_{max}} \dot{\varepsilon}_{eff}^I \qquad (3)$$

where $\dot{\Omega}_{ij}^I$ is the inelastic back stress rate, Ω_{max} is the maximum value of back stress expected, $\dot{\varepsilon}_{eff}^I$ is the effective inelastic strain rate and f_1 is a hardness related material parameter. The effective inelastic strain ε_{eff}^I, is given by:

$$\varepsilon_{eff}^I = \sqrt{\frac{2}{3} \varepsilon_{ij}^I \varepsilon_{ij}^I} \qquad (4)$$

where ε_{ij}^I is the inelastic strain tensor.

The drag stress Z is given by,

$$Z = Z_1 + (Z_0 - Z_1) \exp(-m\varepsilon_{eff}^I) \qquad (5)$$

where Z_0 is the initial value of drag stress, Z_1 is the final value of drag stress and m defines the rate at which Z evolves from Z_0 to Z_1.

From the above set of equations, the following characteristic constants were required to be derived from uniaxial test data: D_0, n, f_1, f_2, Ω_{max}, Z_0, Z_1, m. The determination of these parameters are dependent on a number of mathematical relationships which describe the state variables in terms of material characteristics seen in typical uniaxial tests. These relationships are related to the following material characteristics: saturation of a tensile response curve, the Bauschinger effect, stress relaxation and strain recovery.

The uniaxial form of equations 1 to 4 are utilised in section 7.1 to provide initial estimates of the constitutive state variables, which are then improved upon with the use of a perturbation computer program to arrive at the final set of values, described in section 9.

3. Test Specimens

The specimen design employed for this test series was modified from that used previously at AMRL [9]. These specimens incorporated threads at both ends so that they could be screwed into a set of custom made holding blocks and then inserted into standard testing machine grips. (see Figure 1) The specimens were cylindrical in section and 127mm in length (including threaded ends) with a 9.5mm diameter test section (see Figure 2). There were 10 specimens in total, with each specimen having been previously heat treated to a level consistent with that of the WPF.

It was noted that some of these specimens were slightly distorted as a result of the manufacturing and heat treatment processes. This subsequently affected the alignment process (see Section 8.1).

In order to obtain the most accurate set of results, the alignment of the specimens in the testing machine was paramount. Each specimen was fitted with a set of four strain gauges at ninety degree intervals around the test section. The strain gauges were employed to aid the alignment of the specimens whilst being gripped in the testing machine. They were applied using high temperature cure adhesives to provide the highest bond failure strain. The strain gauges were expected to drift under the application of high strains and their output would be unreliable once the strains reached these high levels (greater than 10,000 $\mu\varepsilon$)[10].

4. Test Equipment

The following testing equipment was used throughout the test series.

- Instron 250 kN universal servo hydraulic testing machine located in the AMRL Fatigue Laboratory.
- Instron Extensometer (Cat no. 2620-602), 25mm gauge length, ± 10% strain range.
- Instron Extensometer (Cat no. 2620-603), 10mm gauge length, ± 10% strain range.
- Mitutoyo Digmatic Indicator (Dial Gauge) (Code no. 543-612), Accuracy 0.02mm @ 20°C.

The 25mm extensometer was placed along the axis of the specimen (see Figure 1) for all of the tests. The 10mm extensometer was also positioned across the centre of the test section, however it was placed 135 degrees around the circumference of the test section with respect to the 25mm extensometer for specimens 3, 6 and 7 only.

Test data were recorded on a PC, using the in-house program ISGAR version 1.85, with each of the following parameters measured:

- Time
- Load (raw voltage)
- Extensometer reading (raw voltage)
- Four strain gauge readings (raw voltage)
- Testing machine LVDT (for initial tests only)

Also during the testing the following real time plots were recorded:

- Load and Extensometer strain vs time on chart recorder
- Load vs Extensometer strain on HP XY plotter.

5. Test Procedure

5.1 Alignment Procedure

Prior to commencement of the testing program each specimen was inspected for any possible distortion due to the heat treatment process. Most of the specimens were found to be slightly bowed, with some showing a more marked effect than others.

Installation of the specimens into the testing machine began with the specimen being screwed into the custom made holders at each end, and the locking nuts attached, but not tightened (see Figure 1). The next step was to clamp the specimen into the top grip of the machine, leaving the bottom end free. By applying a dial gauge to the edge of the top holder the specimen could be approximately aligned in the vertical direction by continually readjusting the top holder. At this point the bottom end of the specimen was clamped and the nuts were tightened. The strain gauge values were recorded and a small compressive strain of -2000 $\mu\varepsilon$, was applied. Any bending of the specimen was observed through the unequal response of the four gauges.

Next, both nuts were loosened and the lower specimen holder was then shimmed in the appropriate direction to remove any apparent bending observed. The process was then repeated until any observed bending effects were minimised. This method was time consuming but accurate, considering that the specimens already possessed a certain degree of bend. This method of aligning the specimens also yielded an accurate estimate of the degree of bending present within a specimen, thus providing a greater understanding of the results.

The final two tests, specimens 6 and 7, were aligned in a different manner due to experience gained from the previous tests. These specimens were first inserted into the machine and the nuts tightened. A small compressive strain was applied and the strain gauge results noted. The specimen was then removed from the machine and then rotated 90 degrees within the holders and then replaced. Again a small compressive strain was applied and the results noted. This was repeated a final time at a rotated

angle of 45 degrees from the initial position. From these three sets of results the bending axis was calculated. The hydraulic grips used only allow alignment in one plane. The specimen was then installed so that its bending axis was in the plane of the testing machine. Specimen distortion is then minimised by shimming the holder in the hydraulic grips.

5.2 Specimen Loading Configuration

The strain ranges for the tests were chosen to simulate the strain levels seen in the FFVH#13 region at 100% CPLT load as given in reference [9]. A symmetric tension / compression load cycle was used to characterise the material, whereas a non-symmetric CPLT cycle was used to represent the actual strain cycle experienced by the FFVH#13 region.

Some materials have shown a non-symmetrical tension and compression monotonic loading response [11]. This phenomenon was investigated in this series of tests. Most uniaxial data is tension oriented only. However, the CPLT cycle involves the initial application of large compressive loads. Therefore it was necessary to investigate both the tension and compression loading regimes.

Previous work has shown that D6ac steel is strain rate independent. Incorporated into the test program was the validation of this material characteristic. The strain rate of $60\mu\epsilon$/sec is representative of the actual CPLT application strain rate and therefore this was used as the baseline.

To fully characterise the material, the unified constitutive model requires a knowledge of stress and strain relaxation. In this test series only the stress relaxation was investigated, in order to evaluate the back stress state variable, Ω (see Section 7.2).

The following is a detailed description of the applied loading and a description of each test specimen.

5.2.1 Specimen No 1: Basic tension/compression cycle at $60\mu\epsilon$/sec

Under extensometer strain control, cycle to $\pm20,000~\mu\epsilon$ tension/compression at a strain rate of 60 $\mu\epsilon$/sec, beginning with the tension cycle (see Figure 3). This test was to investigate the symmetry of a single inelastic strain loop.

5.2.2 Specimen No 2: Basic compression/tension cycle at $60\mu\epsilon$/sec

Repeat test of specimen number 1, however the cycle began with a compression cycle. Again the test was under strain control and at 60 $\mu\epsilon$/sec (see Figure 4). The main aim of this test was to compare the loop shape of a single cycle beginning with a compression application as opposed to that beginning with a tension load.

5.2.3 Specimen No 3: Investigation of specimen bending effects

This test was used to monitor the possible bending effects seen during the previous test sequences. Initially the specimen underwent a number of separate 20,000µε/-20,000µε cycles with two extensometers of differing gauge lengths applied to the test section. After these cycles, a number of tests at increasing symmetric strain levels were conducted to quantify the monotonic saturated stress state for D6ac steel, i.e. the load and strain levels when the stress/strain curve becomes flat. Strain cycles were applied up to 35,000µε/-35,000µε, in increments of ±5,000µε until the specimen failed in compression. This failure was a direct result of the specimen bending out of plane on the compression cycle.

5.2.4 Specimen No 4: Basic tension/compression cycle at 10µε/sec

Under strain control, cycle to ±20,000 µε tension/compression at a strain rate of 10 µε/sec, beginning with the tension cycle (see Figure 5). This test was used to investigate the strain rate sensitivity of D6ac steel.

5.2.5 Specimen No 5: Basic tension/compression cycle at 600µε/sec

Under strain control, cycle to ±20,000 µε tension/compression at a strain rate of 600 µε/sec, beginning with the tension cycle (see Figure 6). This test was used to investigate the strain rate sensitivity of D6ac steel.

5.2.6 Specimen No 6: Stress relaxation under strain control

This test began by applying a tensile loading under strain control at the rate of 60 µε/sec. At 15,000 the strain was held for 2 hours and data recorded initially every second for 3 minutes, then at 20 second intervals. From this point the specimen was loaded up to 20,000 µε and then down to -15,000 Here the strain was held for 2 hours and the stress relaxation was recorded for the compression case every second for 3 minutes then at 20 second intervals. The strain was continued to -20,000 µε and then the specimen was cycled between 20,000 µε and -20,000 µε, until cyclic saturation. (ie. no change in stress/strain loop observed between subsequent cycles) This took approximately five complete cycles. The above process was repeated three times, taking approximately 5 cycles for each loop saturation.

This test was specific to the calculation of the constitutive equation state variables. Although the constitutive relationships realistically only require stress relaxation data on the first cycle for their development, this test provided data on any differences in the stress relaxation levels after applying a cyclic loading.

5.2.7 Specimen No 7: Stress relaxation under strain control

Repeat test of specimen number 6.

7

5.2.8 Specimen No 8: 100% CPLT representative cycle

Apply CPLT cycle (2 cycles of Figure 7) at a constant strain rate of 60 $\mu\varepsilon$/sec.

5.2.9 Specimen No 9: 75% CPLT representative cycle

Apply 75% CPLT cycle (2 cycles of Figure 8) at a constant strain rate of 60 $\mu\varepsilon$/sec.

5.2.10 Specimen No 10: 50% CPLT representative cycle

Apply 50% CPLT cycle (2 cycles of Figure 9) at a constant strain rate of 60 $\mu\varepsilon$/sec.

6. Results and Discussion

The results of this experimental test program were used to determine the state variables for the unified constitutive model (see Section 7.1). The raw data from each specimen are presented in the form of load versus microstrain curves (Figures 10-19), where the microstrain outputs are from the 25mm extensometer unless otherwise noted.

Observations made during the testing program are discussed in detail in the following sections:

6.1 Specimen Alignment

As mentioned previously, the specimens were all slightly distorted, which made accurate specimen alignment extremely difficult from the outset. The specimens were aligned as accurately as possible to ensure bending was kept to a minimum. Most of the tests involved only one or two cycles and therefore it could be assumed that bending effects never progressed to a level which was detrimental to the results. Specimen 3 however, which involved multiple cycle testing, proved susceptible to bending. This can be illustrated by Figure 12, where specimen 3 experienced bending effects after it had undergone a number of continuous cycles. Specimen 3 made use of two extensometers of differing gauge lengths placed at different circumferential positions around the working section. One extensometer of larger gauge length (25mm) controlled the experiment, whilst the second extensometer of smaller gauge length (10mm) was also placed across the centre of the specimen test section, but at 135 degrees around from the larger one. No significant bending occurred within the first few cycles, however after 10 cycles bending of the specimen became obvious. This effect grew as the number of cycles increased. Specimens 6 and 7, which also involved multiple cycle tests, did not produce the same degree of bending as did specimen 3. The bending observed for these specimens was extremely minimal, as both attached extensometers returned the same strain outputs.

Overall, this confirmed that the degree of bending was specimen dependent, and that specimen 3 was the only specimen to exhibit the effects of bending to a significant degree.

6.2 Uniaxial Specimen Design

From the beginning of the testing program it was recognised that the specimen design was not optimum for high tension and compressive testing. The ideal aspect ratio of these types of specimens should be approximately 1.5 [12], which would result in minimal bending and bulging. Bulging was not observed in any of the specimens tested.

The application of the load to the test section could also be improved. The current setup entails the specimen being screwed into a set of high strength tool steel holding blocks and then inserted into the test machine grips. The load is transferred, in shear, through the threaded section of the specimen. Before the testing commenced it was thought that the threads on the specimens might deform under loading and consequently result in an inefficient application of load to the test section. As the test program progressed it was found that the specimen holders threads were deforming. This was discovered through the increasing difficulty in inserting the specimens into the holders as the tests progressed. It is thought that this deformation could be a result of the bending of the specimens implying uneven loads through the threads of the specimen holders, and thus resulting in thread deformation. Considering the extent of thread deformation experienced, it would be beneficial if an alternative gripping technique could be devised for future tests.

In order to determine that the test section would exhibit a uniform stress regime throughout the cross section, an idealised elastic FEM analysis of the specimen was performed. This analysis is detailed in Appendix A and shows that the specimens experienced a constant stress application across the working section.

6.3 Cyclic Saturation

An interesting material characteristic seen throughout all of the multiple cycle tests was the way in which the material cyclically saturated. Most materials take a few cycles to cyclically saturate, however D6ac steel is cyclically saturated after the first cycle. This can be seen in Figures 15 and 16 where, once the material initially yields on the first cycle, the subsequent cycles lie over one another. This effect is consistent throughout all of the multiple cycle tests, tension, compression and CPLT.

6.4 Inelastic Saturation

Another interesting material characteristic observed during the testing was the high level of strain required to reach inelastic saturation (when the stress/strain curve becomes flat). All tests to 20,000 με showed that the material had not inelastically saturated. Furthermore, specimen 3 which reached approximately 35,000 με before failure, clearly did not demonstrate that the material had inelastically saturated. From these data it could be estimated that D6ac steel would inelastically saturate at around 40,000 με.

6.5 Stress Relaxation

In addition to the two separate tests specifically conducted to investigate the stress relaxation properties of D6ac steel, stress relaxation could be seen during every test. Strain control was used for all the tests, and as a result of this, stress (or load) relaxation was observed when a specimen was returned to zero strain at the end of each test. All test results showed the load to relax approximately 30.27 MPa instantaneously upon test completion. If the specimen was left for about 5 minutes, this relaxation progressed to around 56.43 MPa. It is interesting to note that the 2 hour strain holds for the stress relaxation tests showed, on average, a 88.88 MPa load relaxation (see Figures 15 & 16). Figure 20 shows a section of test data for specimen 6 displayed in load time format. The bulk of the stress relaxation occurs within 5 minutes which is seen in all of the tests.

6.6 Bauschinger Effect

The Bauschinger effect, which is the lowering of the absolute value of the elastic limit in compression following a previous tensile loading [11], was prominent throughout all of the tests, as it was for previous D6ac steel tests. Through analysis of a basic symmetric tension/compression strain cycle (Figure 10), it can be seen that D6ac yields quite sharply on the initial yield cycle and then more gradually on subsequent cycles. This effect within itself leads to the occurrence of the Bauschinger effect, as the compression yield following the initial tensile yield is vastly different from that experienced within the initial yield. This phenomenon persists throughout multiple cycle tests (Figures 12,15,16), as the cyclic loops are virtually identical. Previous testing also encountered the Bauschinger effect, which further validates its authenticity as a characteristic of D6ac steel.

6.7 Material Anomalies

Another interesting characteristic displayed by D6ac steel during the cyclic testing was the differing values of Young's Modulus (E) for initial loading and subsequent unload. For a single 20,000/-20,000 με loop beginning with a tension load (see Figure 10), the

Young's Modulus was the same for the initial tension upload and the unload after a compressive load. However, a lower value of E was observed when unloading from any tensile load (see Figures 17,18,19). This phenomenon was quantitatively consistent throughout all of the tests and was exhibited by both extensometer and strain gauges alike. Unloading in the elastic region of the tensile curve did not produce a different value of Young's Modulus, only in unloading after plastic deformation was this characteristic evident.

Another material anomaly observed was the differing maximum load values reached in tension and compression for a symmetric strain cycle application. The maximum load value reached in compression was consistently 10 kN higher than that seen in tension for all of the symmetric tests. Given the associated consistency of the differing values of E, these two characteristics are possibly inter-related.

There exist two possible explanations of these material anomalies. Firstly, if the deformation mechanism of D6ac is slip (most likely mode of deformation) then the cyclic curve and Young's Modulus should be symmetric in tension and compression. In this case the specimens may be bending due to an imperfect alignment, thus causing the differing value of E and maximum load, however the consistency of the results across all of the specimens discounts this theory. It may be possible that slip is not the only deformation mechanism. Grey cast iron is not symmetric in tension and compression and its deformation occurs through mechanisms other than slip [13]. It could be possible that D6ac experiences mechanisms other than slip which results in a non-symmetric response. It is also possible that micro voids could have been introduced into the specimen's structure during heat treatment. As the specimens undergo plastic deformation in the tensile region, the micro voids would be stretched open. Upon load reversal the specimens would effectively possesses a smaller cross sectional area, thus resulting in a decreased value of Young's Modulus. As the specimens are compressed, the micro voids would be closed, resulting in the original Young's Modulus occurring when the specimen unloads from the maximum tension load. The modified Young's Modulus does not occur in the initial tension loading, as the micro voids would only expand out to a significant amount during tensile plastic deformation. This explanation would require a microscopic analysis of the material to confirm the existence of these voids, and thus their effect on the material's behaviour.

7. Constitutive Model State Variable Determination

7.1 Initial Estimation of State Variables

It should be noted that the equations given in this section are used as simplified asymptotic approximations only. Their purpose is to provide a first estimate of the values of the state variables, so that they can be refined to yield an accurate prediction of the material response. Once such an initial estimate of the state variables was obtained they were input into a FORTRAN computer program which contained the

unified constitutive equations 1 to 5. The program was designed to represent the uniaxial test condition under strain control and it allowed the perturbation of the state variables and the subsequent analysis of the response compared to uniaxial test data.

7.1.1 Tensile Response Data

The values of D_0 and n have been selected based upon previous experience for strain rate independent materials [3,8]. At tensile saturation, the back stress is at a maximum, termed Ω_{max}, whilst the drag stress is near it's initial value, Z_0, and remains almost constant. For isothermal conditions the temperature can be omitted from equation 1. Therefore for a saturated uniaxial tensile loading (where σ is at saturation and Ω is a maximum), equation 1 can be re-written in the following form:

$$\dot{\varepsilon}_0^I = \frac{2}{\sqrt{3}} D_0 \exp\left[-\frac{1}{2}\left(\frac{Z_0}{|\sigma_{SAT} - \Omega_{max}|} \right)^{2n} \right] \tag{6}$$

where the term, $\sigma - \Omega / |\sigma - \Omega|$ in equation 1 is equal to +1, and σ_{SAT} is the value of the saturated stress. Inverting equation 6 yields the following which can be used for obtaining a relationship between Ω_{max} and Z_0.

$$\left[-2\ln\left(\frac{\sqrt{3}\dot{\varepsilon}_0^I}{2D_0} \right) \right]^{1/2n} = \frac{Z_0}{\sigma_{SAT} - \Omega_{max}} \tag{7}$$

Here $\dot{\varepsilon}_0^I$ is the initial inelastic strain rate. For a constant strain rate application $\dot{\varepsilon}_0^I$ is equal to the overall strain rate. Therefore from specimen 1 (Figure 10), $\dot{\varepsilon}_0^I = 0.00006$ ε/sec. Substituting this and the relevant values of D_0 and n into equation 7 yields:

$$\left[-2\ln\left(\frac{\sqrt{3}\dot{\varepsilon}_0^I}{2D_0} \right) \right]^{1/2n} = 1.83$$

which leads to the following equation:

$$Z_0 = 1.83\left(\sigma_{SAT} - \Omega_{max}\right) \tag{8}$$

Equation 8 is used later in conjunction with equations 11,12 and 16 to solve for Ω_{max} and Z_0.

7.1.2 Bauschinger Effect

Through analysis of the flow equation 1, it can be seen that the over stress (resultant stress, $\sigma-\Omega$) to produce yield in tension must be the same as the over stress to produce

yield in compression, for constant values of n, D_0 and Z_0. Therefore for the first cycle of a fatigue test when $Z = Z_0$, equation 1 can be rewritten in the following form:

$$\left| \sigma_{yt} - \Omega_{yt} \right| = \left| \sigma_{yc} - \Omega_{yc} \right| \tag{9}$$

where σ_{yt} and σ_{yc} are the values of yield stress for tension and compression respectively. Through analysis of Figure 21 the following two relationships between f_2 and Ω_m can be discerned. (see [8])

$$\Omega_{yt} = f_2 \cdot \sigma_{yt} \tag{10}$$

$$\sigma_{yc} = \Omega_{max} - f_2 \cdot \Delta\sigma \tag{11}$$

From specimen 1 data the following results were extracted:

$\sigma_{yt} = 1340$ MPa
$\sigma_{yc} = -141$ MPa
$\Delta\sigma = 1763$ MPa

Inserting these values into equation 11 leads to the following relationship:

$$-141 \times 10^6 = \Omega_{max} - f_2\left(1763 \times 10^6\right) \tag{12}$$

7.1.3 Saturation Response

Next we make use of the parameter f_1 which describes the inelastic strain to reach saturation, see [8].

$$f_1 = \frac{4.6\Omega_{max}}{\varepsilon_{SAT}^I} \tag{13}$$

where ε_{SAT}^I is the accumulated inelastic strain at the onset of saturation.

7.1.4 Stress Relaxation

Stress relaxation properties can be made use of in the following fashion (see [8]) to relate f_2 to Ω_{max} (see Figure 22).

$$f_2 = \frac{C_1\left[\Omega_{max} - \sigma_B + \sigma_{yt}\right]}{\left|\Delta\sigma_{AB}\right| + C_1\sigma_{yt}} \tag{14}$$

where

$$C_1 = 1 + \frac{2.3|\Delta\sigma_{AB}|}{E\varepsilon^I_{SAT}} \tag{15}$$

From specimen 6 the following data were determined:

$\sigma_B = 1445$ MPa $\qquad \sigma_A = 1535$ MPa

$\sigma_{yt} = 1340$ MPa $\qquad E = 203$ GPa

$\varepsilon^I_{sat} = 40{,}000 \; \mu\varepsilon$

Substituting these values into equations 14 and 15 yields the following equation:

$$(1.0252)\Omega_{max} - (1429 \times 10^6)f_2 = 107 \times 10^6 \tag{16}$$

Therefore solving equations 12 and 16 for f_2 and Ω_{max}:

$\Omega_{max} = 1031 \times 10^6$ MPa

$f_2 = 0.665$

Substituting Ω_{max} into equation 13 yields:

$f_1 = 118.565$ GPa

And finally substituting Ω_{max} into equation 8:

$Z_0 = 1081.53 \times 10^6$ MPa

These values yield an initial estimate of the material constants for the constitutive model.

7.2 Refinement of Initial Predictions

The initial values of the material constants for D6ac steel were refined by comparing the model predictions with symmetric cyclic strain data as well as CPLT cycle data. This produced the final set of constitutive constants listed below.

$\Omega_{max} = 1250$ MPa

$Z_0 = 1081$ MPa

$f_1 = 135$ GPa

$f_2 = 0.585$

The above set of values, are relatively different to the initial estimates calculated using the constitutive relationships. The value of Ω_{max} is larger by about 200 MPa. This is due to the different maximum loads seen during a single tension/compression cycle. As

mentioned in the uniaxial test data discussion, the maximum tension load was consistently about 10 kN lower in comparison to the maximum compression load. The model does not allow for different maximum tension and compression loads and therefore a higher value of Ω_{max} was required to be able to predict an average tension/compression response.

Also the values of f_1 and f_2 are slightly modified with respect to their initial estimations. Basically, these variables control the point at which the material yields and also the approximate strain at which the material saturates. By analysing a symmetric strain cycle for D6ac steel (Figure 10) it can be seen that the material has a very sharp initial yield response. However, after the material has initially yielded, the subsequent cyclic response is quite smooth. Therefore, to be able to predict this vast difference in the initial yield and subsequent yields, the values of f_1 and f_2 were modified accordingly. The variable m, in effect controls the cyclic softening of the material. The final value of 120 was obtained by varying m within the perturbation program until an acceptable response was achieved.

Results of the above state variables can be seen compared to experimental data in Figures 23 and 24.

7.3 Discussion of Constitutive Model Prediction

As can be seen from Figures 23 and 24 the numerical prediction of the material behaviour of D6ac steel is relatively good, however the prediction is erroneous around certain areas of the curve. Examining Figure 23, which depicts a symmetric 20,000 $\mu\varepsilon$/-20,000 $\mu\varepsilon$ loop, the largest discrepancy of the numerical prediction is seen to occur within the reverse yield area, with a maximum difference occurring at around -5000 $\mu\varepsilon$. This large difference can be attributed to the reverse yielding predicted by the numerical model after the compression cycle, compared with the corresponding reverse yield Young's Modulus displayed by the experimental results. As explained earlier the gradient of the elastic unload from tension yield is different from that exhibited within initial loading and unloading from compression yield. This is an uncommon characteristic, and the numerical model is incapable of predicting the correct response. It is also apparent from Figure 23 that the model has difficulty predicting the strain hardening of the material after the initial yield. The model predicts a more gradual yielding than that seen in the uniaxial tests. These limitations coupled with the differing values of Pmax and Pmin, make it impossible to obtain an exact prediction of the material response.

The constitutive model is based theoretically upon the development of the material microstructure consistent with the physical properties of the material. The current formulation of the model is limited in its capability to model the observed inconsistencies in the material response. This limitation would occur with other plasticity models, as the material anomalies displayed by the uniaxial tests do not

agree with the expected material behaviour, and have not been considered in formulating the models.

Another interesting physical characteristic, which leads to the inaccurate prediction of the material response, is the sharp yielding exhibited by D6ac steel on the first yield, as compared with subsequent yields, as can be seen from Figure 23. This is hard for the constitutive model to predict, because the constitutive model is based on a single set of state variables which remain constant throughout the evolution of the material behaviour. This excludes the variables Z_1 and Z_0 which describe the upper and lower bounds of the drag stress, and evolve throughout the material deformation. Other variables, such as f_1 and f_2, for example, which describe the evolution of the back stress, Ω_m, do not evolve.

Basically, the terms f_1 and f_2 control the yield point of the material. In general, the larger the value of f_1 the higher the stress reached before the onset of yield, whilst the higher the value of f_2, the lesser the value of strain whereby the material saturates. The opposite effects are also true. If f_1 and f_2 were the only controlling mechanisms of the material yield, then the same shape of yield for the initial loading, and for subsequent cyclic loading would be experienced, however this is not the case. The hardening parameters f_1 and f_2 effectively combine with the evolving value of the drag stress, Z, which thus leads to the alleviation of the sharp yield effect seen for the initial loading.

However, there seems to exist a limit to which these parameters can combine to produce a smooth transition from initial yield to cyclic yield. As can be seen in Figures 23 and 24, the constitutive model cannot predict the initial yield point and then accurately predict the extremely gradual yield depicted by the experimental data for the cyclic loading. This is because the only variable that evolves from the initial yield to the cyclic yield is the drag stress. The values of f_1 and f_2 remain constant.

During the development of the constitutive material constants it was found that one set of variables gave an excellent match of the initial yield, with a poor prediction of the cyclic response, whilst a second set of constants grossly misrepresented the initial yield, but gave an excellent prediction of the cyclic response (see Figures 25 and 26). The largest difference in the values of the variables between the two scenarios was shown by the hardening variables f_1 and f_2. It could be inferred that an evolution in the value of the variables f_1 and f_2 within the model between the initial yield and the cyclic condition could improve the overall numerical prediction. In effect the changes to the hardening variables would not be evolutionary, rather a one off shift of the values after the material has initially yielded. This would allow the constitutive model to give a better overall prediction of the material behaviour, as it would accurately model the initial yield as well as the cyclic condition.

Another material characteristic exhibited by D6ac steel, which is not accurately predicted by the constitutive model, is the relaxation of the mean stress during a cyclic loading application. This can be most effectively seen for a CPLT comparison between the experimental results and the numerical prediction as in Figure 24. The mean stress

relaxation is a direct result of the maximum compressive stress approaching the maximum tensile stress in magnitude as the material progresses cyclically. During cyclic loading the maximum tensile stress remains constant whilst the maximum compressive stress relaxes, thus reducing the mean stress of each progressive cycle. Most unified constitutive models can accurately predict the main cyclic development of a given material, however, they become inadequate when it comes to the modelling of mean stress relaxation under strain control, or conversely, strain shakedown or ratcheting under stress (load) control [14,15]. Shakedown is the stabilisation of the mean strain under cyclic loading, whilst ratcheting is the divergent behaviour of the mean strain as the number of cycles increases.

As we are mainly concerned with a strain controlled loading (CPLT), mean stress relaxation is of interest whilst shakedown and ratcheting are not analysed. Basically, the modelling of mean stress relaxation is a direct response of the application of kinematic hardening within the model. A linear kinematic hardening rule does not predict any mean stress relaxation. Whilst the application of a non-linear kinematic hardening rule does predict mean stress relaxation, it most commonly results in an over prediction [15]. As can be seen from the numerical results (Figure 24) the Stouffer constitutive model over predicts the mean stress relaxation which is a common trait of such a constitutive model. Therefore, it is unrealistic to expect the constitutive model to accurately predict the stress relaxation exhibited by D6ac steel, without modification to the application of the hardening rule. This type of modification would require re-formulation of the constitutive equations.

It should be noted that the afore mentioned shortfalls of the unified constitutive model apply purely to the material behaviour of D6ac steel. The tests revealed a unique combination of material properties which are uncommon and unexpected for this type of high strength steel. Consequently, these anomalies cannot be effectively predicted by the Stouffer constitutive model, or any other plasticity modelling technique. Apart form the small discrepancies which can be viewed in Figures 23 and 24, the constitutive model predicts the cyclic nature of the D6ac steel well. The CPLT loading cycle is of a non-symmetrical nature and therefore it is more difficult to predict, especially by classical plasticity techniques. So although the unified constitutive model does not provide an exact representation of the behaviour of D6ac steel, it does predict the cyclic response to a degree which is acceptable for its application to the F-111 DADTA process.

8. Conclusions

This report has described the development of material constants of D6ac steel for the unified constitutive model. Test data was obtained through a serious of uniaxial tests and an initial prediction of the material constants was obtained. These initial predictions were refined using a computer representation of the model to arrive at a final set of values.

During the development of the material constants a number of material anomalies were observed which could not be predicted by the model. These anomalies were peculiar to this type of steel, and were therefore not able to be handled by the unified model. New testing techniques were also developed for uniaxial specimens which led to the reduction of out of plane bending effects.

Overall a set of material constants were produced which allowed the cyclic prediction of the material behaviour of D6ac steel. These results are to be applied to the calculation of the residual stress field in the F-111 WPF undergoing a CPLT load application.

9. References

1) Watters, K., Paul, J. and Searl, A., 'AMRL Support for RAAF F-111 ASIP', Aeronautical and Maritime Research Laboratory, DSTO, Melbourne, Australia, December 1995.

2) Lillingston, K., 'F-111 Wing Variable Sweep Strain Survey', Airframes and Engines Division, Aeronautical and Maritime Research Laboratories, Structures Laboratory Report No. 8/95, DSTO, Melbourne, Australia, August 1995.

3) Stouffer, D.C. and Bodner, J.R., 'A Relationship between Theory and Experiment for a State Variable Constitutive Equation', ASTM, STP-765, 239-250, DSTO, Melbourne, Australia, 1982.

4) Paul, J., 'Final Report on the Implementation of a Constitutive Model into the PAFEC Finite Element Package', Airframes and Engines Division, Aeronautical and Maritime Research Laboratories, DSTO, Melbourne, Australia, November 1996. (In Press)

5) Bridgford, N., 'A Summary of the Bodner-Stouffer Constitutive Model', Aeronautical Research Laboratories, TM-513, DSTO, Melbourne, Aust, May 1989.

6) Williams, J. F., Jones, R., Stouffer, D. C., Bridgeford, N., Kuruppu, M., Paul, J., 'The Elastic-Plastic Behaviour of 7050-T7451 Aluminium', University of Melbourne, Department of Mechanical and Manufacturing Engineering, Internal Report No. SM/1/90.

7) Paul, J., Bridgford, N. and Stouffer, D., 'Progress Report on Implementation of a Constitutive Model into the PAFEC Finite Element Package', Aeronautical Research Laboratories, Struct-TM-529, DSTO, Melbourne, Aust, June 1990.

8) Stouffer, D.C. and Dame, L.T., 'Inelastic Deformation of Metals: Models, Mechanical Properties, and Metallurgy', John Wiley & Sons, 1996.

9) Molent, L., Swanton, G., 'F-111 Fuel Flow Vent Hole #13 Strain Surveys', Aeronautical Research Laboratories, TN-33, DSTO, Melbourne, Aust, June 1993.

10) Allan, R. B., 'Loading of an Elongated Hole Coupon to Determine Strain as a Function of Load and Compressive Buckling Load of Coupon', Aeronautical and Maritime Research Laboratories, DSTO, Melbourne, Aust, January 1996. (In Press)

11) Lemaitre, J and Chaboche, J.L., 'Mechanics of Solid Materials', Cambridge University Press, 1990.

12) Matic, P., Kilby, G.C., Jolles, M.I., 'The Relationship of Tensile Specimen Size and Geometry Effects to Unique Constitutive Parameters for Ductile Materials', Mechanics of Materials Branch, Material Science and Technology Division, October 1987.

13) Wang, C.H. and Brown, M.W., 'Modelling of the Deformation Behaviour of Flake Graphite Iron Under Multi-Axial Cyclic Loading', Journal of Strain Analysis, Vol 29, No 4, 277-288, 1994.

14) Chaboche, J.L., 'Modelling of Ratcheting: Evaluation of Various Approaches', Mecamat '92: Multiaxial Plasticity, 1-4 Sept. 1992.

15) Ohno, N and Wang, J.D., 'Kinematic Hardening Rules for Simulation of Ratcheting Behaviour', Mecamat '92: Multiaxial Plasticity, 1-4 Sept. 1992.

16) Yakushev, A.I., 'Effect of Manufacturing Technology on the Strength of Threaded Connexions', Oxford, Pergamon, 1964.
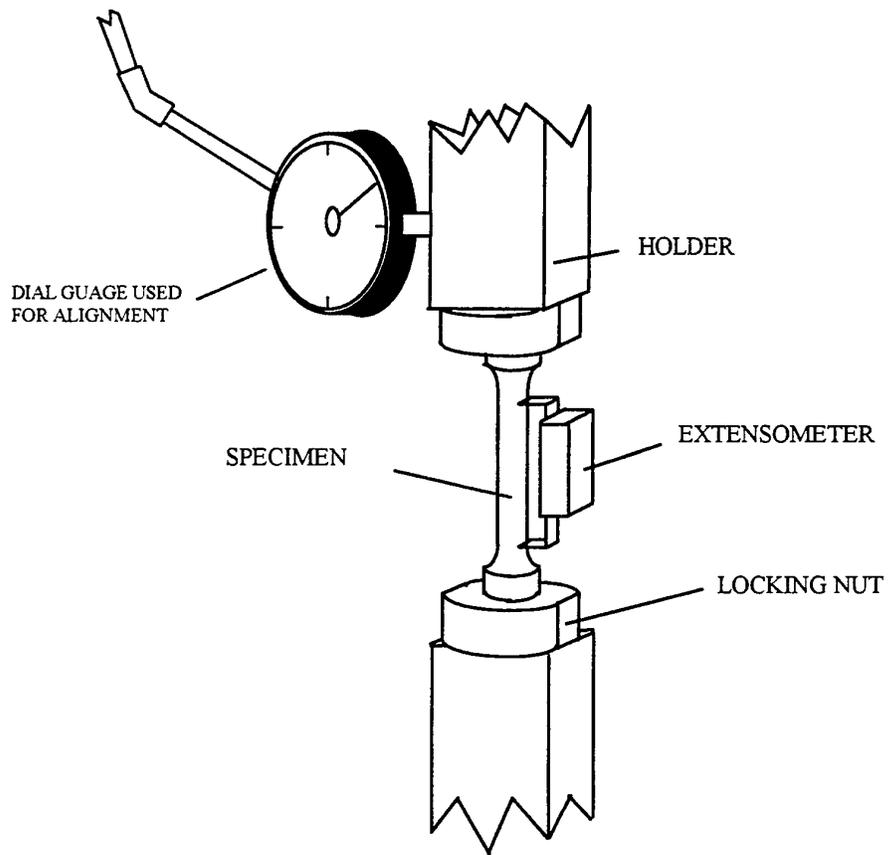
Figure 1.   *Experiment Test Configuration*
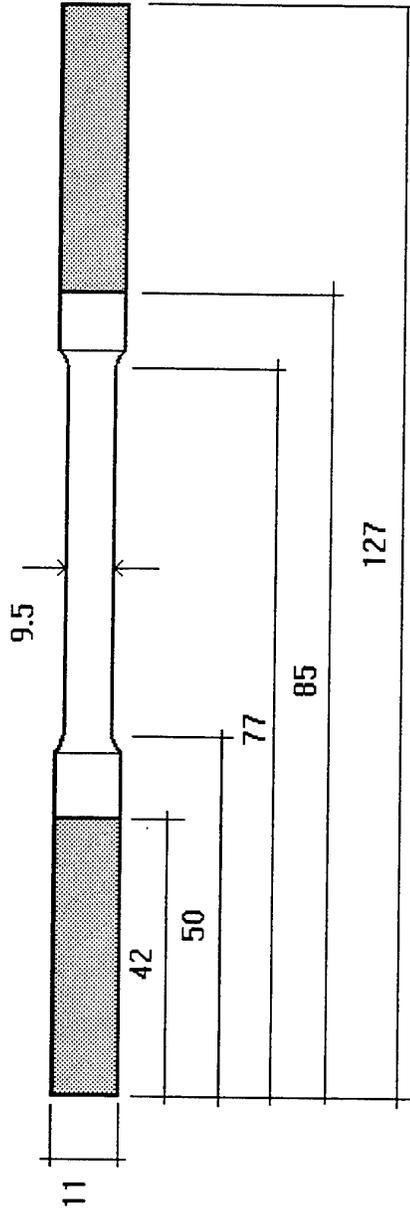
Figure 2. *Uniaxial Test Specimen (dimensions in mm)*
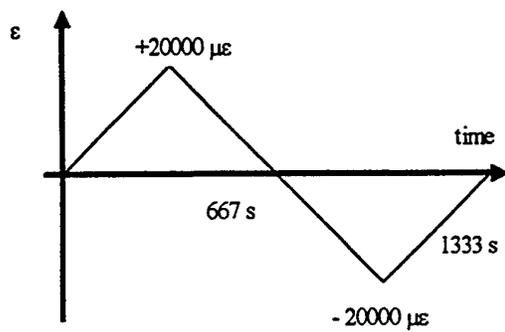
Figure 3.   Tension/Compression cycle to 20,000 $\mu\varepsilon$
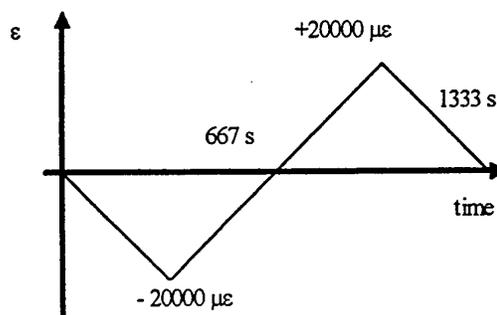
Figure 4.   Compression/Tension cycle to 20,000 $\mu\varepsilon$
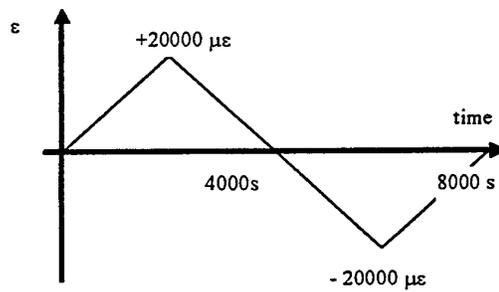
Figure 5.   Tension/Compression cycle to 20,000 $\mu\varepsilon$ at 10 $\mu\varepsilon$/sec
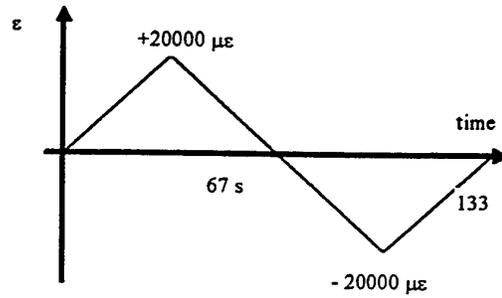
Figure 6.   *Tension/Compression cycle to 20,000 $\mu\varepsilon$ at 600 $\mu\varepsilon$/sec*
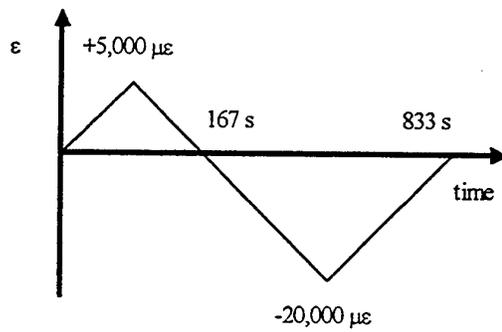
Figure 7.   *100% CPLT cycle*
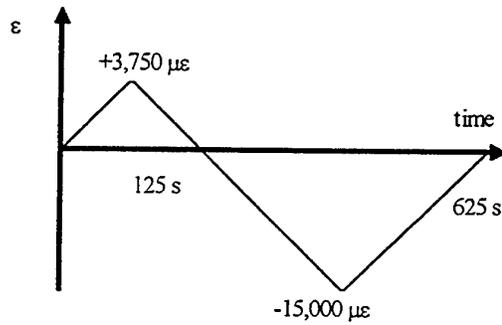
Figure 8.   *75% CPLT cycle*
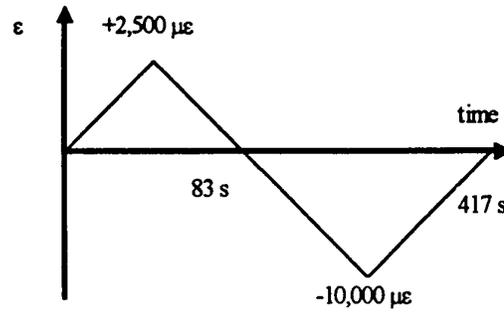
Figure 9. *50% CPLT cycle*
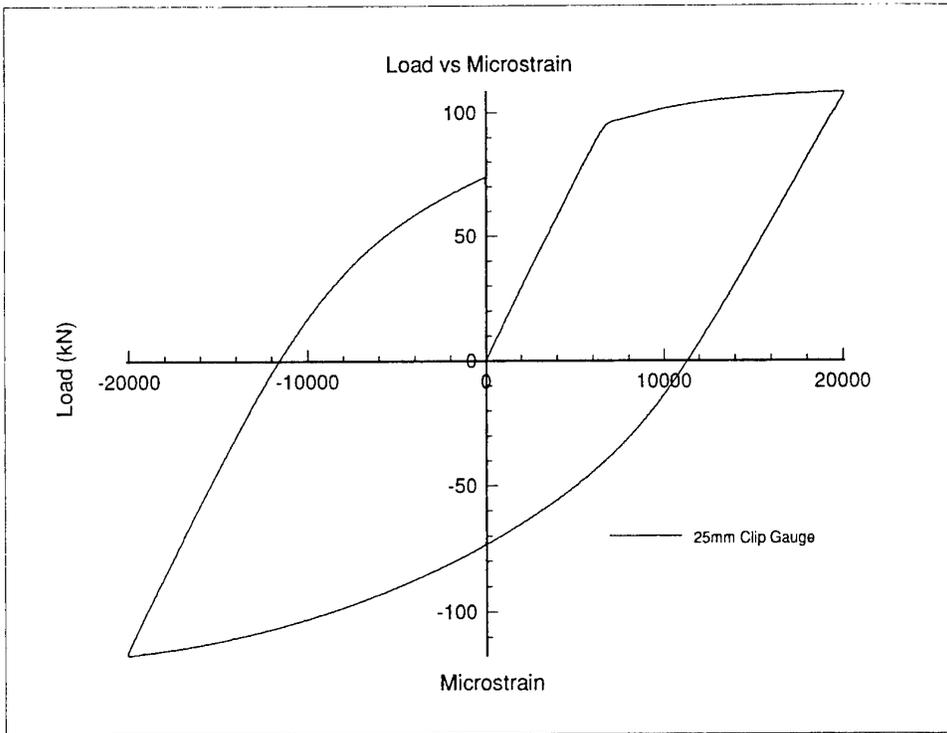
Figure 10. Specimen 1 (60 microstrain/sec)
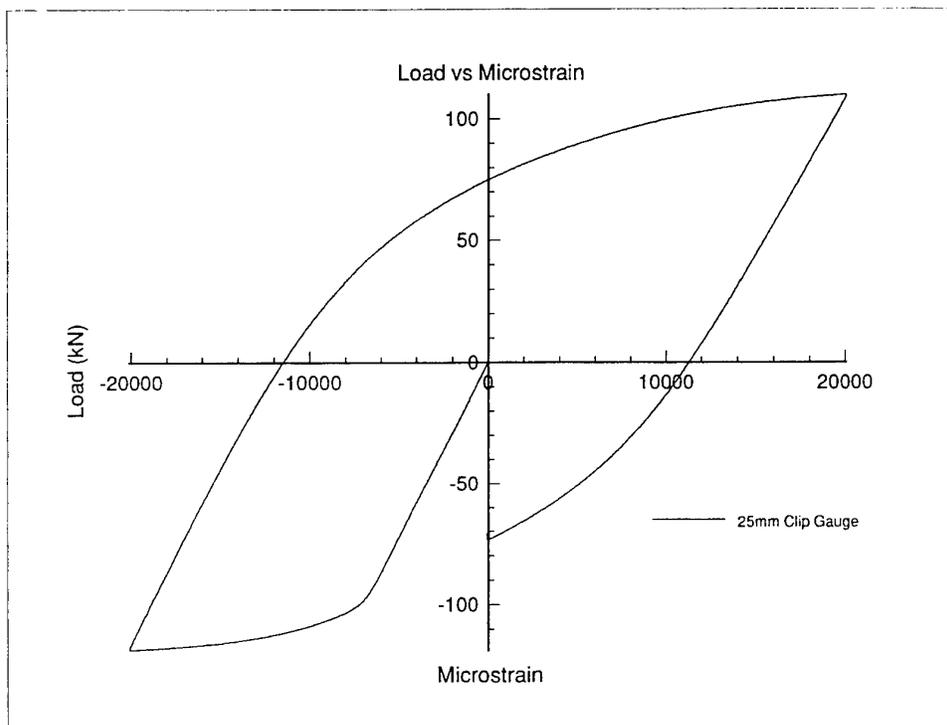
Figure 11. Specimen 2 (60 microstrain/sec)
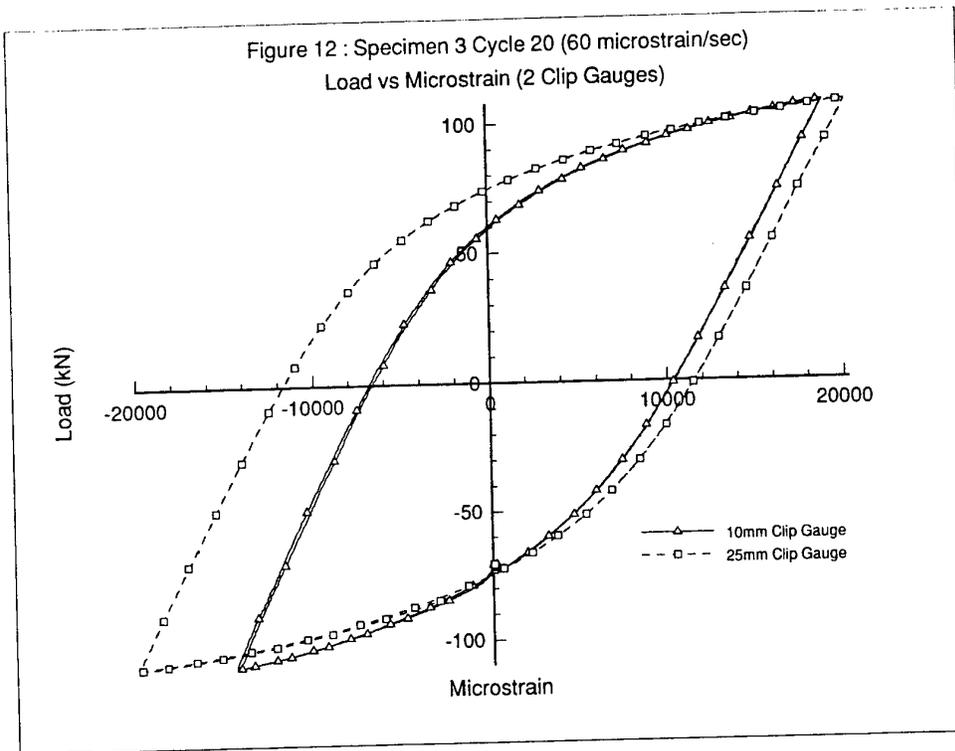
Figure 12.   Specimen 3 Cycle 20 (60 microstrain/sec)
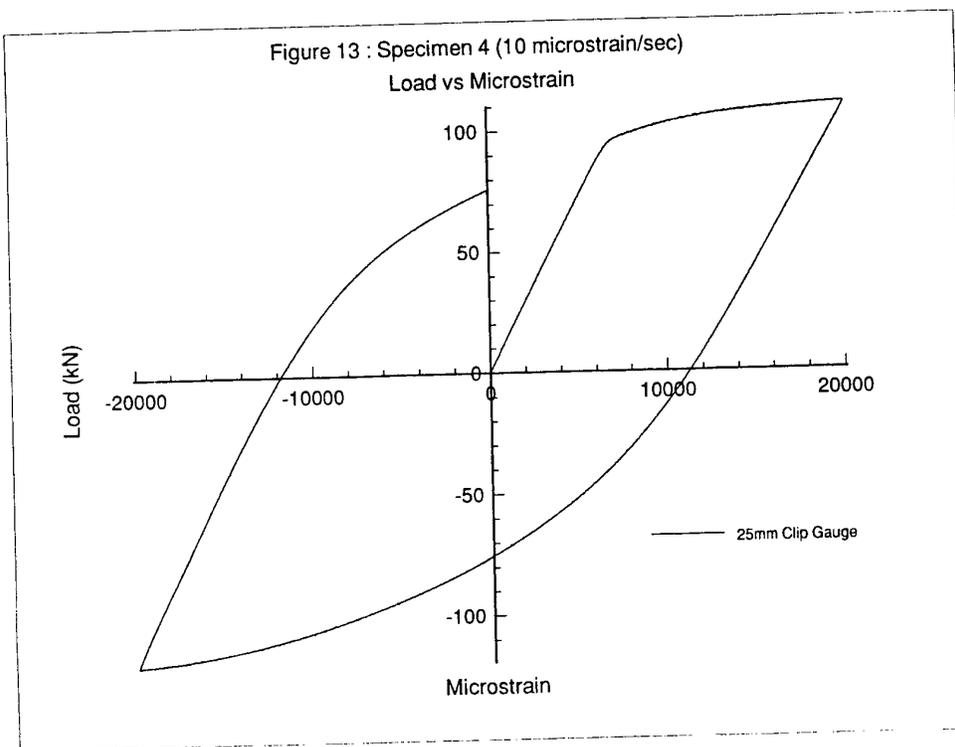
Figure 13.   Specimen 4 (10 microstrain/sec)
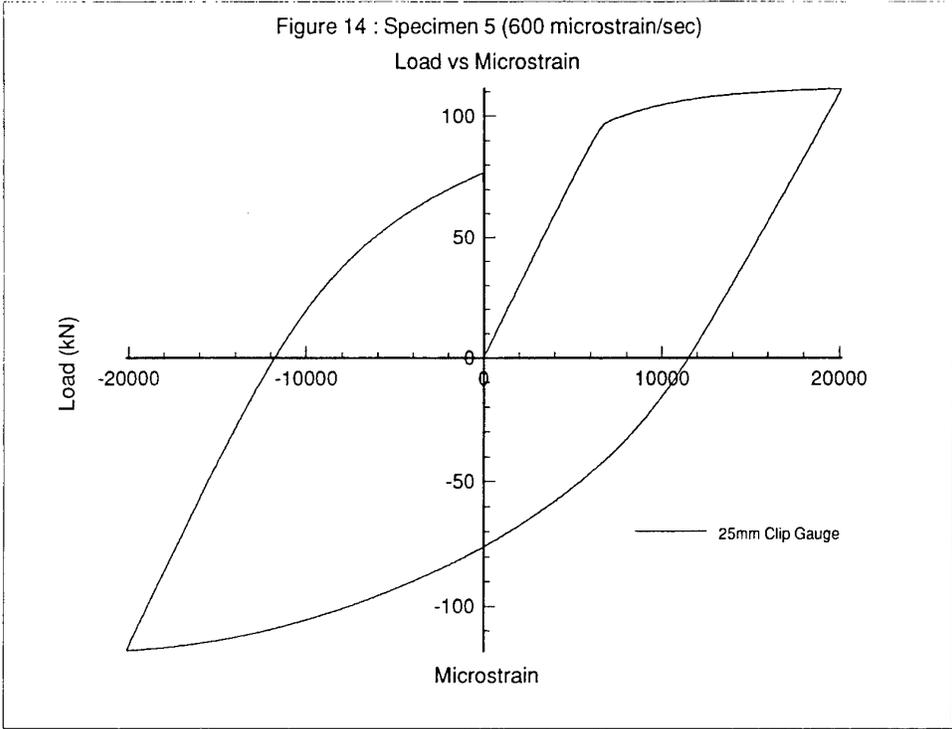
Figure 14.   Specimen 5 (600 microstrain/sec)
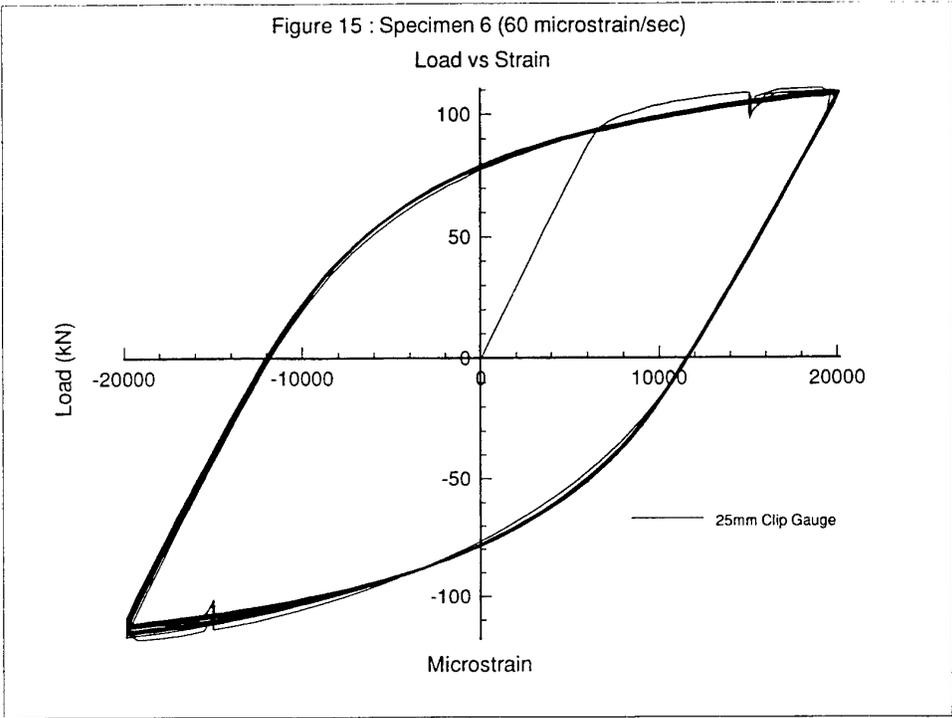
Figure 15.   Specimen 6 (60 microstrain/sec)

Figure 16 : Specimen 7 (60 microstrain/sec)
Load vs Strain
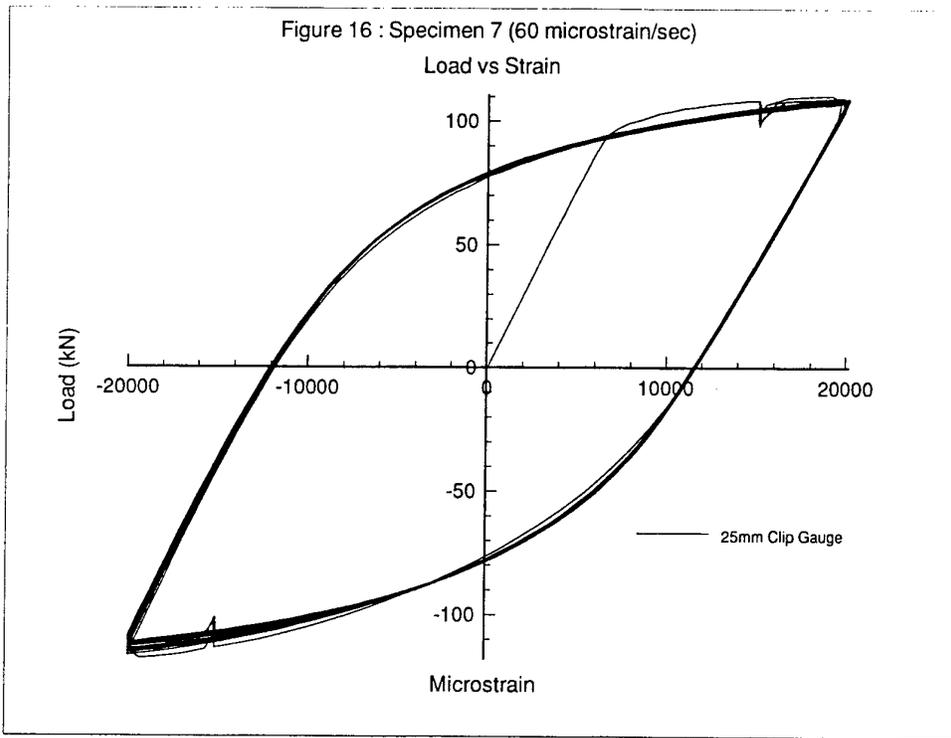
Figure 16. Specimen 7 (60 microstrain/sec)

Figure 17 : Specimen 8 100% CPLT (60 microstrain/sec)
Load vs Microstrain
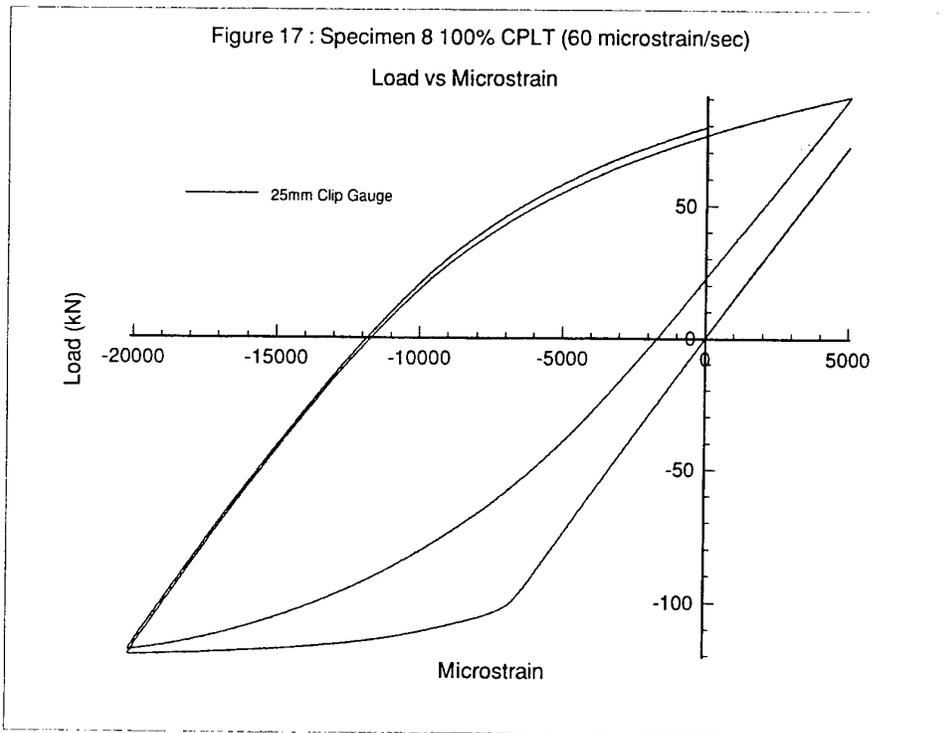
Figure 17. Specimen 8 100% CPLT (60 microstrain/sec)

Figure 18 : Specimen 9 75% CPLT (60 microstrain/sec)

Load vs Microstrain
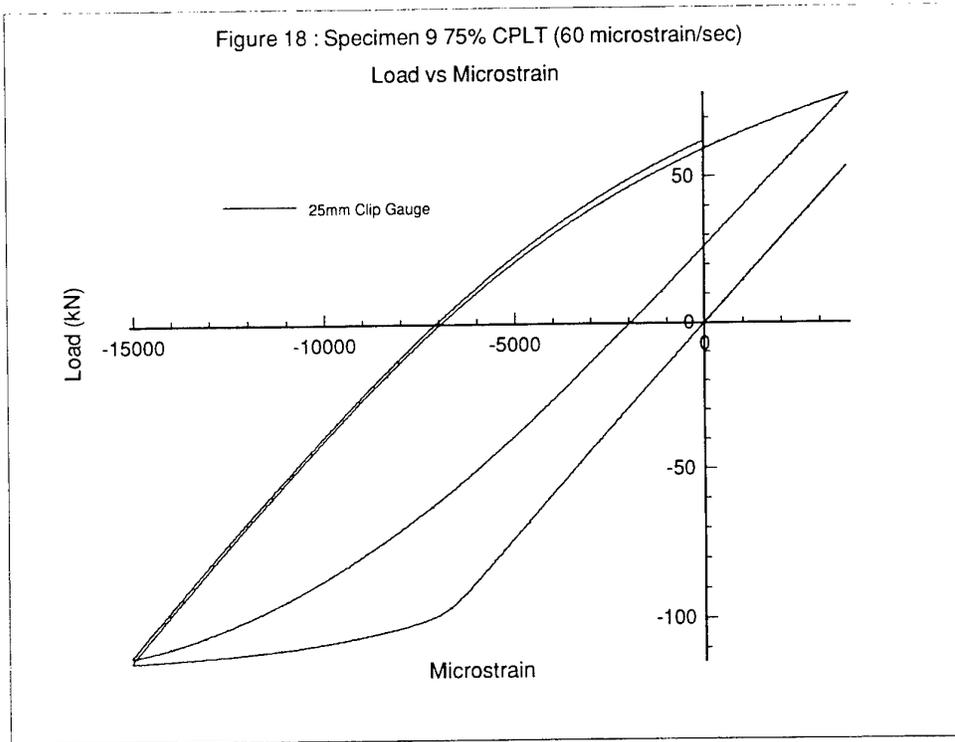
Figure 18.   Specimen 9 75% CPLT (60 microstrain/sec)

Figure 19 : Specimen 10 50% CPLT (60 microstrain/sec)

Load vs Strain
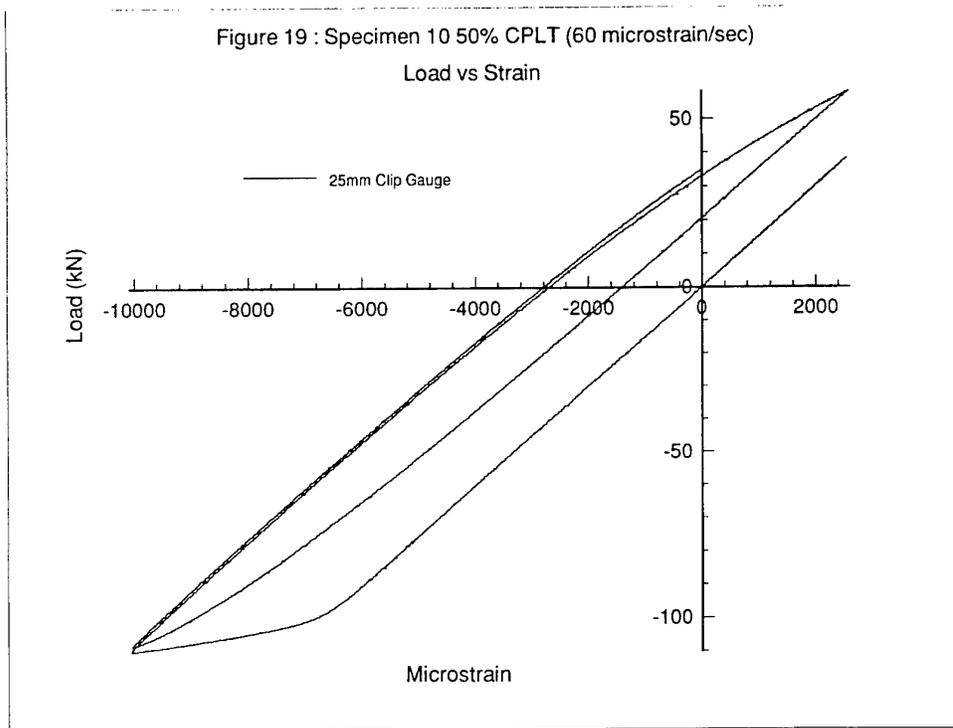
Figure 19.   Specimen 10 50% CPLT (60 microstrain/sec)
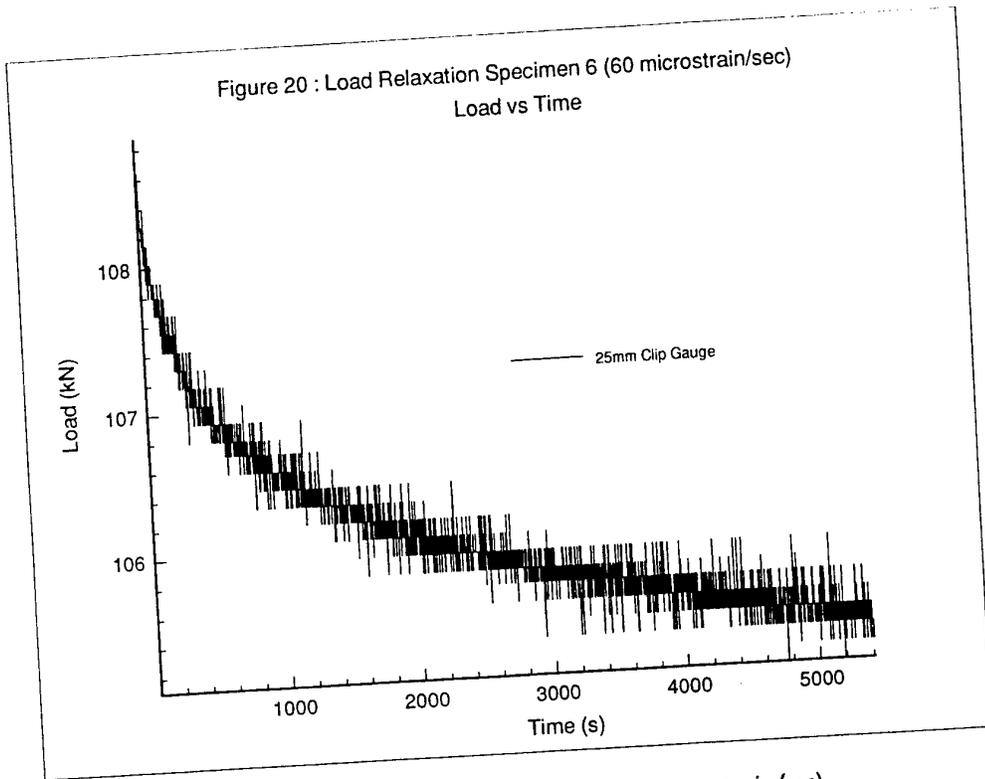
Figure 20. *Load Relaxation Specimen 6 (60 microstrain/sec)*
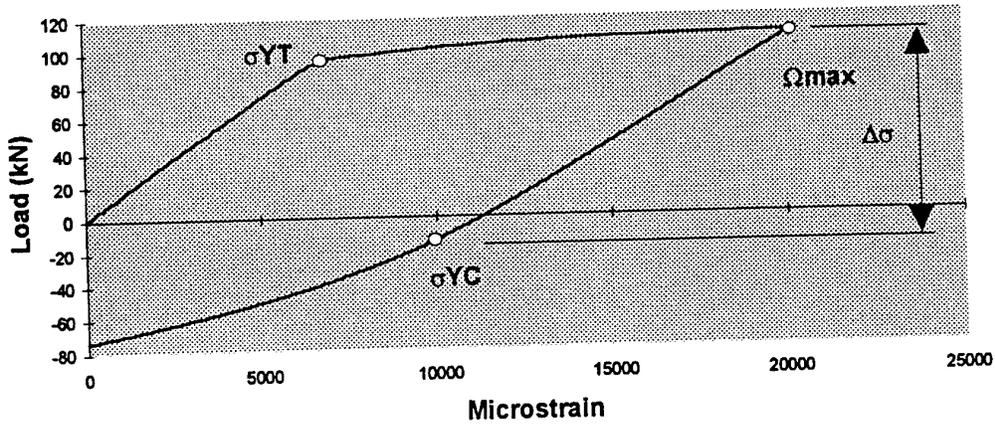
Figure 21.   Bauschinger Effect
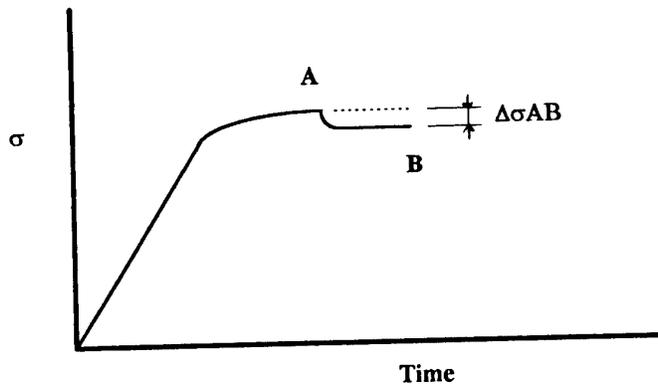
Figure 22.   Stress Relaxation Calculation
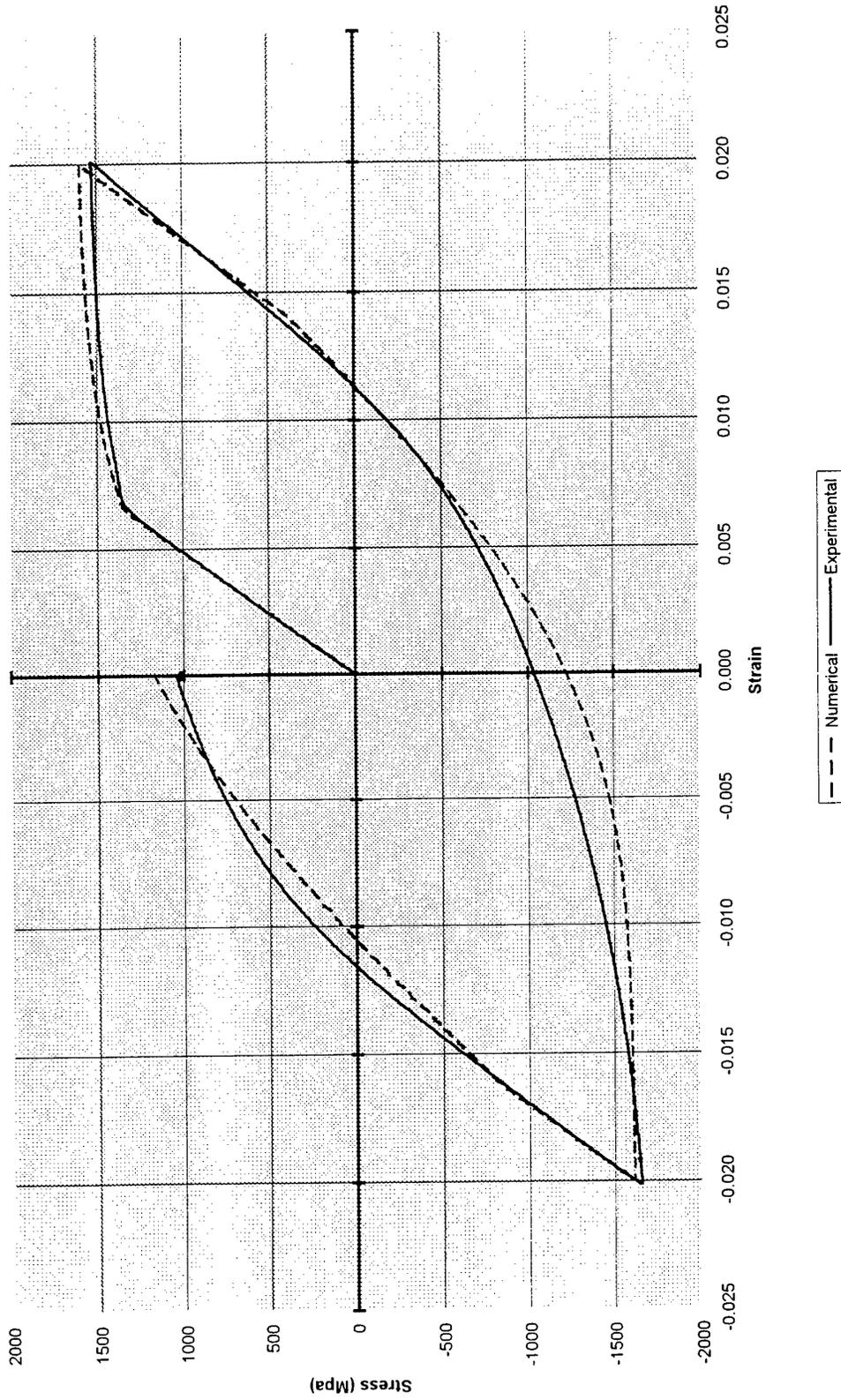
Figure 23. Comparison of Numerical and Experimental Cyclic Response

Figure 24 : Comparison of Numerical
and Experimental CPLT Response
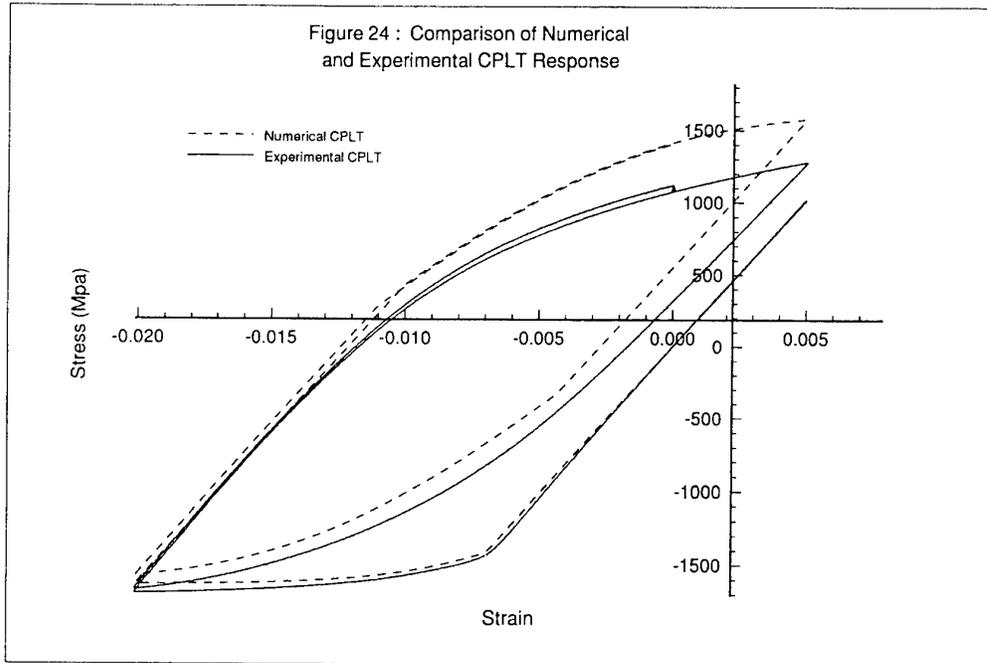
Figure 24.   Comparison of Numerical and Experimental CPLT Response

Figure 25 : COMPARISON OF NUMERICAL AND EXPERIMENTAL
RESPONSE FOR MONOTONIC CONSTANTS

Z0=347 Mpa
Z1=347 Mpa
f1=30000 Mpa
f2=0.865
OMmax=1510 Mpa
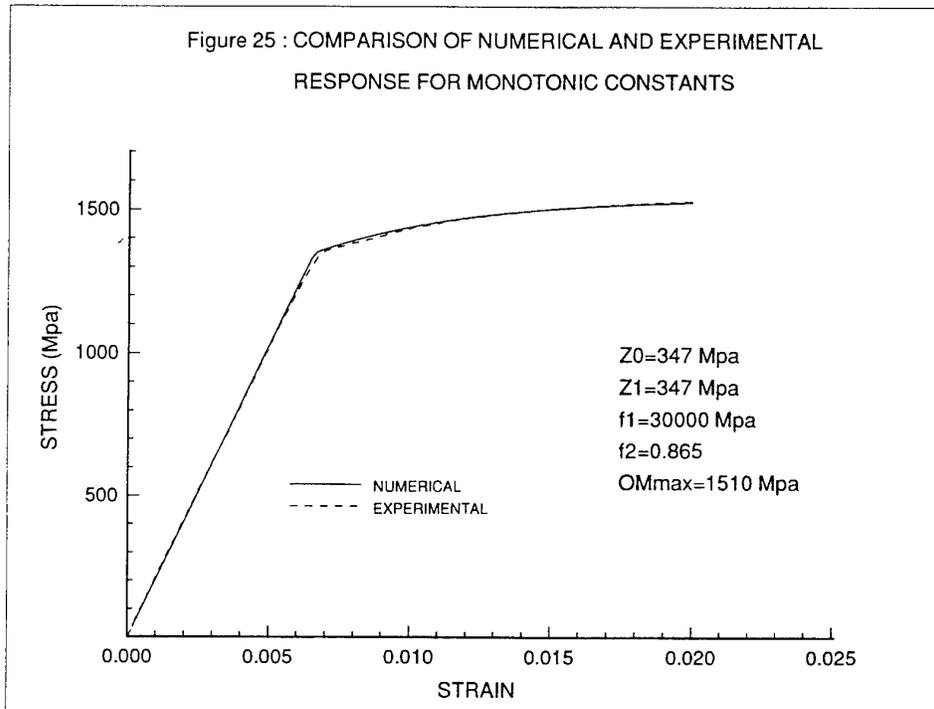
Figure 25.   Comparison of Numerical and Experimental Response for Monotonic Constants

Figure 26 : Comparison of Numerical and Experimental
Response for Cyclic Constants

Z0=1081 Mpa
Z1=300 Mpa
f1=115000 Mpa
f2=0.565
OMmax=1510 Mpa
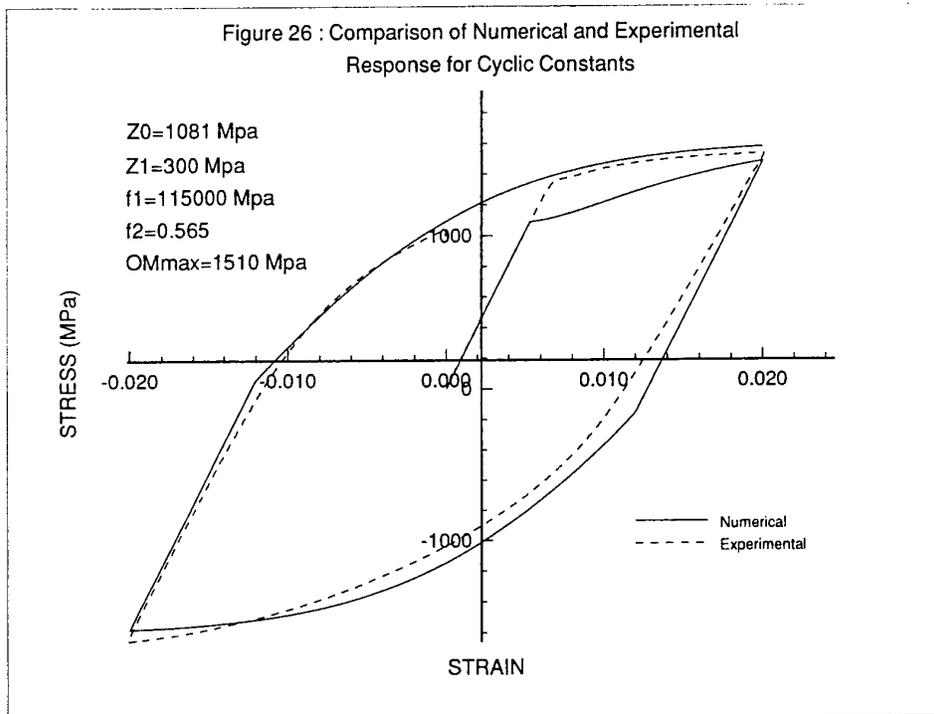
Figure 26.   Comparison of Numerical and Experimental Response for Cyclic Constants

Appendix A:

Uniaxial Specimen Finite Element Model

A1. Introduction

The specimens used to calculate the unified constitutive state variables were made of D6AC steel, cylindrical, with a length (including threads) of 127mm and a test section diameter of 9.5mm (see Figure 2). All of the tests were conducted in strain control. The controlling extensometer (25mm gauge length) was attached across the test section which was 27mm in length. A fillet curve exists at the junction between the working section and the threaded region. Given that the overall test section length and the gauge length are quite close, and that the knife edges of the extensometer sit extremely close to the fillet, a stress analysis of this region was performed to investigate any possible interference to the extensometer.

To analyse the stress distribution within the specimen a detailed finite element model was constructed. The model consisted of the specimen only and was aimed at providing details of the transfer of load from the threaded connections through to the test section. In addition, the through thickness stress distribution of the specimen was examined. It was anticipated that high regions of stress would appear at the section change between the threaded area and the test section, whilst the stress in the test section would be constant.

The initial distortion of the specimen due to machining and heat treatment has been ignored in the analysis.

A2. Finite Element Model Description

The finite element model of the uniaxial specimen was produced using the PAFEC Finite Element Package currently in use at AMRL. The model contained 4483 nodes, 720 20-noded isoparametric brick elements, 360 15-noded isoparametric prism elements and 13,041 degrees of freedom. A uniform mesh was employed with increased detailed meshing throughout the working section of the specimen (see Figure A1). The model was restrained at one end and loaded at the other, thus simulating the way in which the specimen was loaded in the testing machine. To simulate the correct level of restraint, the nodes around the periphery of the threaded area were restrained in all directions thus emulating a clamped end. The loading of the opposite end was applied as a distributed tensile load.

The general application of load is performed by varying the distribution along the threaded end whereby most of the load is applied to the first few threads and then

rapidly diminishes along the remaining length of the thread. For this model a mathematical estimate of this distribution was employed which was based around the following equation:

$$P(z) = \frac{Pm}{\sinh(mH)}\cosh(mz) \qquad \text{(A1)}$$

where p(z) is the force taken up by the zth turn of the thread, P is the total load acting along the thread, m is a coefficient dependant upon the construction of the thread, and H is the length of engagement [16].

The model was loaded with a equivalent distributed axial tensile load of 110kN. Although the specimen experiences plasticity at this level of loading, a plastic analysis was not performed. The loading was applied as point loads around the periphery of the threaded section of the specimen, with the longitudinal distribution conforming with that previously discussed.

A3. Results

As expected the highest regions of stress were found to exist in the fillet radius where the two sections meet, occurring at the beginning of the working section. The stress plots (Figure A2) depict the surface stress distribution throughout the specimen, and highlight the maximum stress occurring at the radial section change. Figure A2 is a plot of stress in the longitudinal direction. The resulting elastic stress concentration factor at the surface of the specimen was calculated to be 1.2. Figure A3 is a plot of a section cut through the middle of the specimen. It can be seen in this plot that the areas of maximum stress exist around the periphery of the specimen and do not propagate through the thickness. From this plot it is also interesting to note that the specimen achieves a constant through the thickness loading throughout the length of the test section.

A4. Conclusion

The results of this analysis clearly show that the uniaxial specimen experiences a constant through the thickness loading throughout the working section. In addition, it can be seen that localised areas of high stress exist at the section change. As this is where the clip gauge knife edges sit, it is possible that the clip gauge may be reading slightly inconsistent results. However, since the localised stress intensity factor is 1.2, and the stress distribution is uniform across the working section, it is anticipated that the effect on the experimental data would be negligible.

PLASTIC

ROTATION
X = 34
Y = 26
Z = 14
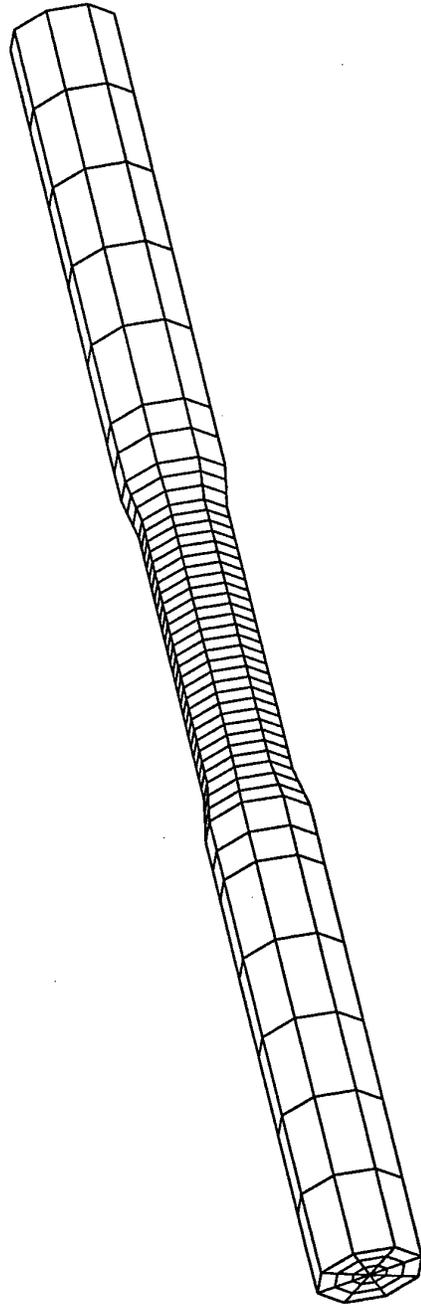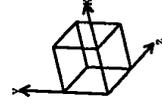
Figure A1. Uniaxial Finite Element Mesh

39

LINEAR
STATICS
LOAD CASE   1

ROTATION
X =   34
Y =   26
Z =   14

LOAD   1
SIGXX
CLIP   5
M SURF
MAX STR
POWER   3
2.38
MIN STR
POWER   1
-    0.84

E 2
22.60
20.21
17.81
15.44
13.05
10.66
8.27
5.88
3.49
1.11
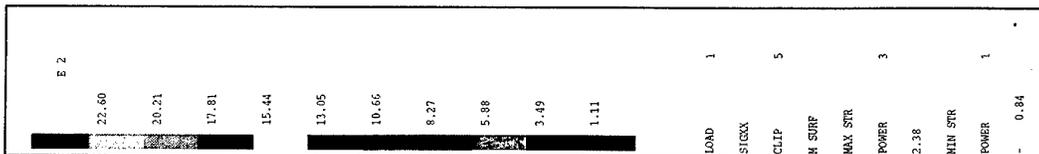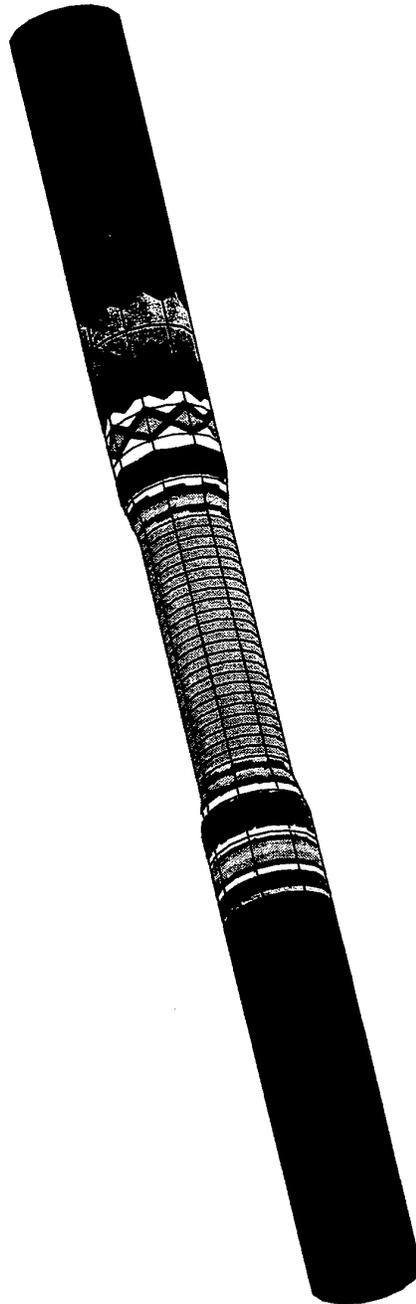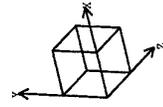
Figure A2.   Tension Load (110kN) Stress Distribution
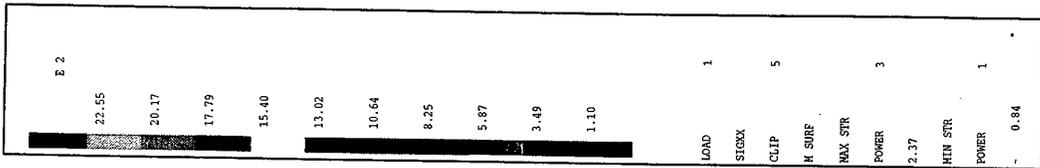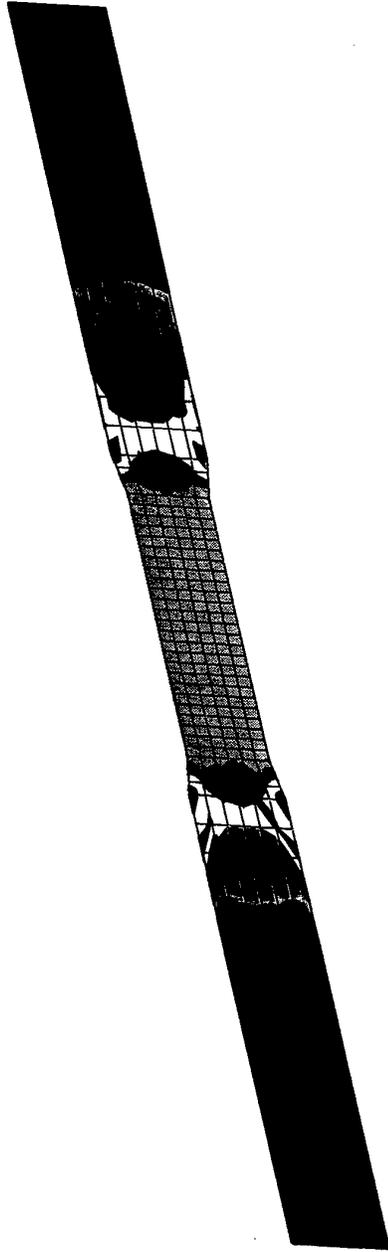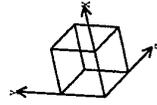
Figure A3. Tension Load (110kN) Stress Distribution X-Section

Characterisation of D6AC Steel Using A Unified Constitutive Model

A.Searl and J. Paul

AUSTRALIA

1. DEFENCE ORGANISATION

a. **Task Sponsor**   DTA-LC

b. **S&T Program**
Chief Defence Scientist
FAS Science Policy   } shared copy
AS Science Corporate Management
Director General Science Policy Development
Counsellor Defence Science, London (Doc Data Sheet)
Counsellor Defence Science, Washington (Doc Data Sheet)
Scientific Adviser to MRDC Thailand (Doc Data Sheet)
Director General Scientific Advisers and Trials/Scientific Adviser Policy and
    Command (shared copy)
Navy Scientific Adviser (Doc Data Sheet and distribution list only)
Scientific Adviser - Army (Doc Data Sheet and distribution list only)
Air Force Scientific Adviser
Director Trials

Aeronautical and Maritime Research Laboratory
Director
Chief of Airframes and Engines Division
F. Rose
K. Watters
N. Swansson
A. Searl (5 copies)
J. Paul (5 copies)
C. H. Wang
R. Allan

DSTO Library
Library Fishermens Bend
Library Maribyrnong
Library Salisbury (2 copies)
Australian Archives
Library, MOD, Pyrmont (Doc Data sheet only)

c. **Capability Development Division**
Director General Maritime Development (Doc Data Sheet only)
Director General Land Development (Doc Data Sheet only)
Director General C3I Development (Doc Data Sheet only)

e. **Army**
   ABCA Office, G-1-34, Russell Offices, Canberra (4 copies)

f. **Air Force**
   ASI2A

g. **Intelligence Program**
   Defence Intelligence Organisation
   Library, Defence Signals Directorate (Doc Data Sheet only)

i. **Corporate Support Program (libraries)**
   OIC TRS, Defence Regional Library, Canberra
   Officer in Charge, Document Exchange Centre (DEC), 1 copy
   *US Defence Technical Information Centre, 2 copies
   *UK Defence Research Information Center, 2 copies
   *Canada Defence Scientific Information Service, 1 copy
   *NZ Defence Information Centre, 1 copy
   National Library of Australia, 1 copy

2. **UNIVERSITIES AND COLLEGES**

   Australian Defence Force Academy
       Library
       Head of Aerospace and Mechanical Engineering
   Deakin University, Serials Section (M list), Deakin University Library, Geelong, 3217
   Senior Librarian, Hargrave Library, Monash University
   Librarian, Flinders University

3. **OTHER ORGANISATIONS**

   NASA (Canberra)
   AGPS

OUTSIDE AUSTRALIA

4. **ABSTRACTING AND INFORMATION ORGANISATIONS**
   INSPEC: Acquisitions Section Institution of Electrical Engineers
   Library, Chemical Abstracts Reference Service
   Engineering Societies Library, US
   Materials Information, Cambridge Scientific Abstracts, US
   Documents Librarian, The Center for Research Libraries, US

5. **INFORMATION EXCHANGE AGREEMENT PARTNERS**
   Acquisitions Unit, Science Reference and Information Service, UK
   Library - Exchange Desk, National Institute of Standards and Technology, US
   National Aerospace Laboratory, Japan
   National Aerospace Laboratory, Netherlands

SPARES (10 copies)

Total number of copies: **69**

DEFENCE SCIENCE AND TECHNOLOGY ORGANISATION DOCUMENT CONTROL DATA	1. PRIVACY MARKING/CAVEAT (OF DOCUMENT)

2. TITLE Characterisation of D6AC Steel Using A Unified Constitutive Model	3. SECURITY CLASSIFICATION (FOR UNCLASSIFIED REPORTS THAT ARE LIMITED RELEASE USE (L) NEXT TO DOCUMENT CLASSIFICATION) Document (U) Title (U) Abstract (U)

4. AUTHOR(S) A.Searl and J. Paul	5. CORPORATE AUTHOR Aeronautical and Maritime Research Laboratory PO Box 4331 Melbourne Vic 3001

6a. DSTO NUMBER DSTO-TR-0556	6b. AR NUMBER AR-010-282	6c. TYPE OF REPORT Technical Report	7. DOCUMENT DATE July 1997

8. FILE NUMBER M1/8/982	9. TASK NUMBER AIR96/102	10. TASK SPONSOR DTA-LC	11. NO. OF PAGES 22	12. NO. OF REFERENCES -

13. DOWNGRADING/DELIMITING INSTRUCTIONS None	14. RELEASE AUTHORITY Chief, Airframes and Engines Division

15. SECONDARY RELEASE STATEMENT OF THIS DOCUMENT

Approved for public release

OVERSEAS ENQUIRIES OUTSIDE STATED LIMITATIONS SHOULD BE REFERRED THROUGH DOCUMENT EXCHANGE CENTRE, DIS NETWORK OFFICE, DEPT OF DEFENCE, CAMPBELL PARK OFFICES, CANBERRA ACT 2600

16. DELIBERATE ANNOUNCEMENT

No Limitations

17. CASUAL ANNOUNCEMENT	Yes

18. DEFTEST DESCRIPTORS

finite element analysis, plastic deformation, stress relaxation, F-111C aircraft

19. ABSTRACT
An experimental test program was undertaken to characterise the inelastic response of D6ac steel under differing cyclic loading. A unified constitutive model was used to describe material behaviour. Constants for the model were extracted from the test results and numerical model predictions were compared with the experimental results. The tests revealed that D6ac steel saturates after one cyclic loop and a change in modulus was observed after unloading from a tensile load. Also described are improvements in the testing of uniaxial specimens, focusing on techniques for specimen alignment to minimise out of plane bending effects.